

Frictional behavior of large displacement experimental faults

N. M. Beeler,¹ T. E. Tullis, M. L. Blanpied,¹ and J. D. Weeks²

Department of Geological Sciences, Brown University, Providence, Rhode Island

Abstract. The coefficient of friction and velocity dependence of friction of initially bare surfaces and 1-mm-thick simulated fault gouges ($< 90 \mu\text{m}$) of Westerly granite were determined as a function of displacement to $>400 \text{ mm}$ at 25°C and 25 MPa normal stress. Steady state negative friction velocity dependence and a steady state fault zone microstructure are achieved after $\sim 18 \text{ mm}$ displacement, and an approximately constant strength is reached after a few tens of millimeters of sliding on initially bare surfaces. Simulated fault gouges show a large but systematic variation of friction, velocity dependence of friction, dilatancy, and degree of localization with displacement. At short displacement ($<10 \text{ mm}$), simulated gouge is strong, velocity strengthening and changes in sliding velocity are accompanied by relatively large changes in dilatancy rate. With continued displacement, simulated gouges become progressively weaker and less velocity strengthening, the velocity dependence of dilatancy rate decreases, and deformation becomes localized into a narrow basal shear which at its most localized is observed to be velocity weakening. With subsequent displacement, the fault restrengthens, returns to velocity strengthening, or to velocity neutral, the velocity dependence of dilatancy rate becomes larger, and deformation becomes distributed. Correlation of friction, velocity dependence of friction and of dilatancy rate, and degree of localization at all displacements in simulated gouge suggest that all quantities are interrelated. The observations do not distinguish the independent variables but suggest that the degree of localization is controlled by the fault strength, not by the friction velocity dependence. The friction velocity dependence and velocity dependence of dilatancy rate can be used as qualitative measures of the degree of localization in simulated gouge, in agreement with previous studies. Theory equating the friction velocity dependence of simulated gouge to the sum of the friction velocity dependence of bare surfaces and the velocity dependence of dilatancy rate of simulated gouge fails to quantitatively account for the experimental observations.

Introduction

Experimental faults that slide at a steady state velocity equal to the remote loading rate can exhibit an unstable response if loading rate or stress is changed. The physical processes leading to instability in laboratory samples may also be responsible for the nucleation of earthquakes on natural faults [Brace and Byerlee, 1966]. Instability (stick-slip sliding), which results from the interaction between the strength of the fault surface and the elastic surroundings, arises when fault strength μ decreases with slip δ at a rate greater than the elastic stiffness $k (= d\mu / d\delta)$ of the surroundings. Typically, the strength of bare rock surfaces depends negatively on the log of slip velocity ($d\mu_{ss} / d\ln V < 0$, velocity weakening) [Dieterich, 1978, 1979; Tullis and Weeks, 1986]. This negative rate dependence permits instability when the fault is embedded in compliant surroundings. Instability is favored by more negative values of $d\mu_{ss} / d\ln V$ and by low values of k [Dieterich, 1979; Rice and Ruina, 1983; Gu et al., 1984].

Shearing of significant amounts of rock flour (simulated gouge) of identical composition to the rock surfaces used in initially bare experiments often results in more stable sliding as was

first noted by Byerlee and Summers [1976]. In studies where friction velocity dependence was measured at very short displacement ($<3 \text{ mm}$), friction of simulated gouge depends positively on the log of slip velocity ($d\mu_{ss} / d\ln V > 0$, velocity strengthening), a property which precludes instability at all values of k [Tullis, 1988]. The observed stabilizing effect of gouge has led to speculation that the presence of gouge explains the absence of earthquakes on faults at shallow depths in the Earth [Marone and Scholz, 1988; Marone et al., 1991]. However, experimental evidence of the stabilizing effect of gouge is not definitive, because displacement dependence of friction velocity dependence is sometimes observed. For example, Dieterich [1981] showed that samples with dry simulated granite gouge can undergo a transition from velocity strengthening to velocity weakening within the first few millimeters of slip. Such a transition in the friction velocity dependence of quartz gouge is seen by Marone and Kilgore [1993] but is not seen by Solberg and Byerlee [1984] in experiments to 5 mm displacement on dry simulated granite gouge or by Marone et al. [1990] in experiments to 13 mm displacement in quartz gouge under wet, drained conditions. Even more complicated displacement dependence is seen in dry, super fine quartz simulated gouge which undergoes transitions from stable to unstable sliding and back to stable sliding within the first 5 mm of displacement [Wong et al., 1992]. Since natural faults undergo many orders of magnitude more slip than experimental faults, understanding the origin of displacement dependence of friction velocity dependence is of great importance in extrapolating the experimental results to the Earth.

Although previous studies have offered explanations of the stabilizing effect of gouge, experimental results to date are am-

¹Now at U.S. Geological Survey, Menlo Park, California.

²Now at WaveMetrics Inc., Lake Oswego, Oregon.

biguous. Two explanations have been offered as to why gouges are more stable than initially bare surfaces. First, *Biegel et al.* [1989] speculated that stabilization in gouge is due to an enhanced degree of grain fracture in gouge. They suggest that the friction velocity dependence of grain fracture is positive so that if more fracture occurs in gouge than in bare surface experiments, the friction velocity dependence will be more positive. Second, in the most thorough experimental study, *Marone et al.* [1990] proposed that enhanced velocity strengthening in gouge is due to a contribution to friction from dilational work against normal stress. This explanation is theoretically based and supported by experiments on saturated, drained, thick (4 mm) layers of quartz gouge. Recent measurements by *Marone and Kilgore* [1993] also show a qualitative correlation between changing thickness and friction velocity dependence but do not quantitatively adhere to the prediction of *Marone et al.* [1990].

The original motivation for this study was to test the hypothesis put forth by *Tullis and Weeks* [1986] that the differences between the friction velocity dependence of gouges and bare surfaces observed in short displacement experiments were an artifact of the initial conditions. They predicted that with sufficient displacement, the friction velocity dependence measured for initially bare surfaces and simulated gouge would converge to a single characteristic value. Furthermore, they hypothesized that the characteristic friction velocity dependence would be velocity weakening. In this study the displacement dependence of friction and velocity dependence of friction to displacements greater than 400 mm were determined for both initially bare surfaces and simulated gouges of Westerly granite at room temperature and 25 MPa normal stress. Initially bare surfaces were found to have a constant negative friction velocity dependence at displacements greater than 18 mm. The presence of simulated gouge on an experimental fault was found to increase the friction velocity dependence over that observed for initially bare surfaces, at all displacements, in agreement with the results of *Byerlee and Summers* [1976] and *Marone et al.* [1990] at shorter displacement and somewhat different normal stress. Thus neither prediction of *Tullis and Weeks* [1986] has been borne out by the experiments, and the results are more complex than initially anticipated. For layers of simulated gouge, the friction velocity dependence, frictional resistance, gouge microstructure, and changes in gouge thickness depend on displacement in a complicated way, but all vary in a related, systematic fashion. Analysis of the data shows that the stabilizing effect of gouge can not be explained quantitatively by dilational work. Alternative explanations, such as additional deformation processes operating within the gouge, may still be required to account for the difference in friction velocity dependence between gouges and bare surfaces.

Experimental Procedures

Sliding experiments were conducted on paired rings of Westerly granite in a high-pressure, computer-interfaced rotary shear apparatus [*Tullis and Weeks*, 1986]. Four initially bare surface samples were slid to different displacements up to 479 mm, and five samples with simulated gouge were slid to displacements up to 407 mm. Microstructural observations from an additional 16 experiments (5 bare surface, 11 simulated gouge) which support the results of this study are summarized in the results section, although the mechanical results of these experiments are not included due to technical problems at large displacements.

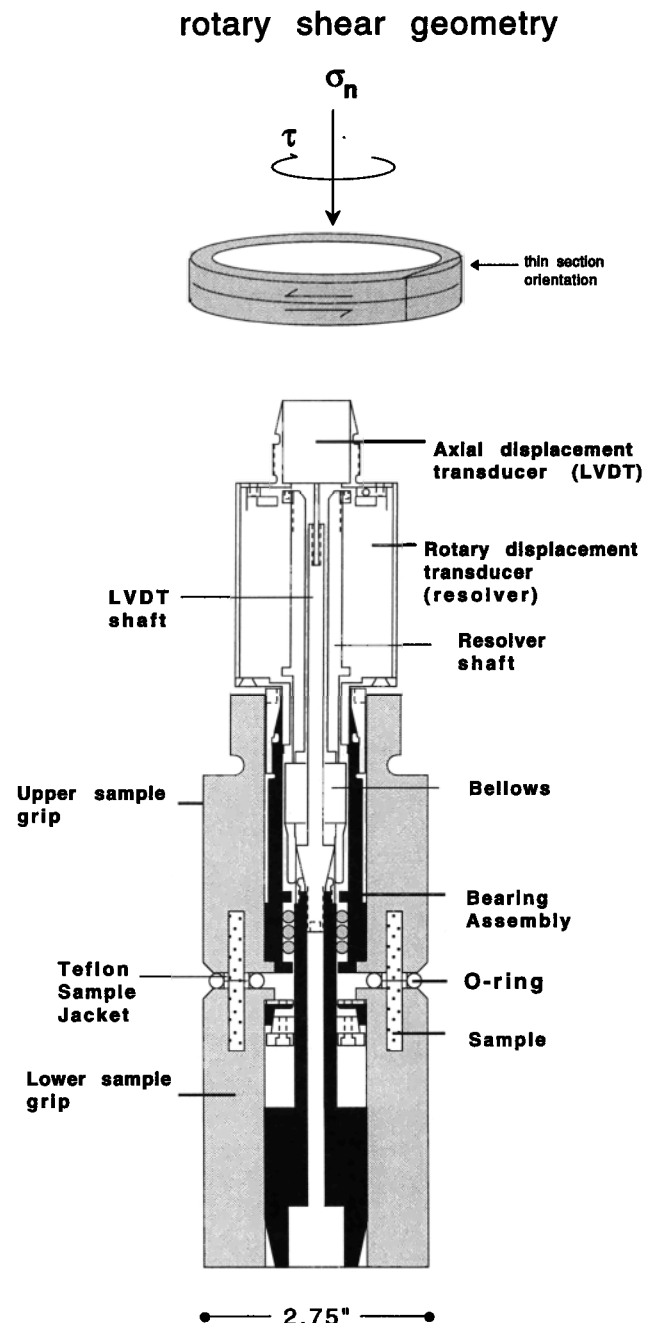


Figure 1. The experimental rotary sliding geometry. During sliding the upper ring remains fixed, and the lower ring rotates. Confining pressure is applied to the sample via two O-rings and four Teflon rings which lie directly against the rock. Thin sections are cut in the orientation shown.

Sample Assemblies

The assembly used is similar to that described by *Tullis and Weeks* [1986] with some modification to allow more precise measurements of slip displacement and fault thickness. All experiments were done in rotary shear (Figure 1); the upper sample grip is held fixed, and the lower grip is rotated by a steel piston (not shown); this piston also transmits an axial load. A sliding, gas-tight jacket of Teflon rings and O-rings excludes the confin-

ing medium (nitrogen gas). The Teflon rings remain fixed to the upper and lower sample rings and slide against one another. The upper sample ring is vented to the atmosphere to prevent the buildup of pore pressure in case of a jacket leak. The vent is monitored for leaks by a bubbler tube. The normal stress on the sliding surface results from the combination of the confining pressure and the axial load. The outer diameter of the sliding surface is 53.98 mm, the inner diameter is 44.45 mm and the area of contact is 735 mm². Attached to each of the sample grips are bearing races which contain alignment ball bearings. The bearings allow axial and rotary motion but prevent misalignment of the samples. Axial and rotary displacements can be recorded simultaneously, allowing determination of changes in gouge thickness with displacement.

Sample Preparation

Sample rings were cored from blocks of Westerly granite (the "blue" variety, from Westerly, Rhode Island). The granite is homogeneous with an average grain size of 0.75 mm, a density of 2.646 g/cm³, and a porosity of 1.1%. Modal analysis [Brace et al., 1965] shows that it is made up of 28% quartz, 35% microcline, 32% plagioclase (An₁₇), 5% mica (biotite plus minor muscovite), and <1% magnetite, other opaque minerals, and hydrous silicate alteration products. The rock rings were epoxied into hardened steel grips and were ground to height with a surface grinder. Surface finish was applied by grinding with #60 (250 μm) SiC grit on a glass plate, resulting in a centerline average roughness of 0.01 mm [Power et al., 1988]. Surface preparation of the rock was performed at room temperature and humidity. In simulated gouge experiments, rock rings (forcing blocks), prepared identically, were used to transmit normal force and torque to the gouge.

Simulated gouge, provided by J. Byerlee, was prepared by crushing Westerly granite and passing the fragments through standard sieves. Gouge not passing the sieves was recrushed until all of it would pass a #170 sieve (88 μm), and all size fractions passing the sieve were retained for use. Gouge was applied to the lower sample surface between the Teflon rings, smoothed to the desired thickness, and then lightly tamped to reduce the initial porosity under room humidity conditions. An initial porosity of ~55% prior to application of confining pressure was determined by measuring the mass and initial thickness of gouge. The amount of gouge used was chosen to result in a ~1.0 mm thick layer when compacted under load.

Experiments

At the start of an experiment, confining pressure was raised to 21 MPa and servo-controlled on a 1/2 s cycle to within the measurement precision of 0.05 MPa. Axial load was then raised to bring the normal stress to 25 MPa. Axial load was servo-controlled, generally to within the measurement precision of 0.07 MPa. Both shear stress (torque) and axial load were measured with a combined load and torque cell located within the pressure vessel. Constant rate loading was provided by an electrohydraulic stepping motor. All velocity and displacement values given in this paper are circumferential and are calculated for the radial midline of the sliding surface (radius of 24.5 mm); due to the finite width of the surface, these quantities vary radially by up to 10% of the quoted values. A full rotation of the lower sample corresponds to 153.6 mm of slip. The shear stiffness *k* of the

loading column between the motor and the sliding surface, normalized by the normal stress of 25 MPa, is about 0.002 μm⁻¹.

Experimental Measurements

Data were recorded digitally at fixed time intervals, with a maximum frequency of 10 samples/s. Measurements were obtained simultaneously for gas pressure, axial load, torque, room temperature, displacement (rotation angle) and the length of the loading column.

Friction

Shear stress and normal stress were computed from the measured pressure, axial load, and torque using the known area of the sliding surface, and the coefficient of friction was calculated as the ratio of shear stress to normal stress. This resulted in values of μ having a resolution of 3 x 10⁻⁴ at 25 MPa normal stress.

Friction Velocity Dependence

To a first approximation, rock frictional strength, measured by shear resistance τ, is proportional to normal stress σ_n (τ = μ σ_n) [Byerlee, 1978]. Although frictional strength at constant normal stress can be simply described by the coefficient of friction μ, sliding stability during slip at constant normal stress is determined principally by small changes in friction that occur in response to changing conditions of slip rate [Dieterich, 1978, 1979]. The characteristic response of rock friction to changes in sliding velocity consists of two apparently additive, log velocity-dependent effects: a positive, instantaneous dependence (direct effect) and a negative dependence which evolves with displacement (evolution effect) (Figure 2). An empirical constitutive law based on the original relations of Dieterich was developed by Ruina [1983] to describe the friction of initially bare surfaces:

$$\tau = \sigma_n \mu = \sigma_n \left[\mu_0 + a \ln(V/V_0) + b \ln(\theta V_0/D_c) \right] \quad (1)$$

where *a*, *b*, μ₀, and *D_c* are experimentally determined constants, *V* is the slip velocity, θ (state variable) is a function which depends on time and displacement, and *V₀* is the velocity at which the steady state friction is μ₀. The state variable has the dimensions of time and at steady state θ_{ss} = *D_c* / *V*. By substitution into (1), the steady state friction velocity dependence is

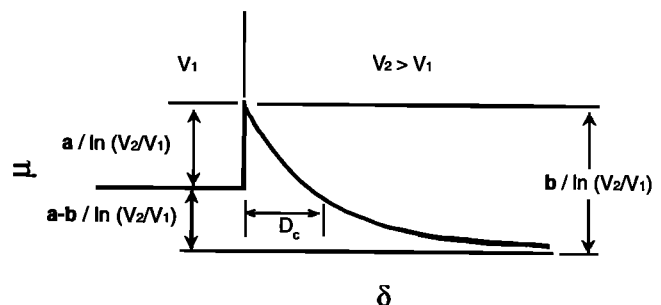


Figure 2. Frictional behavior of constitutive equation (1) as a function of displacement for a step-wise increase in sliding rate for an infinite value of loading stiffness. The velocity step results in an instantaneous direct effect of magnitude *a*ln*V* / *V*₀, followed by an exponential decay of magnitude *b*ln*V*₀ / *V* to a new steady state level. The characteristic displacement of the exponential evolution function θ is *D_c*. The net change in steady state friction is (*a* - *b*)ln*V* / *V*₀. Velocity weakening frictional behavior is shown.

$$d\mu_{ss} / d\ln V = a - b \quad (2)$$

and can be determined by experimental measurement of μ_{ss} at two different sliding velocities (Figure 2).

The value of $d\mu_{ss} / d\ln V$ was measured by alternating the loading velocity between 1 and 10 $\mu\text{m/s}$. Velocity was held constant usually for at least 500 μm to allow friction to evolve to a new steady state value. In most experiments, a standardized sequence of velocity steps between 1 and 10 $\mu\text{m/s}$ was performed, with a slip displacement of 1, 5, or 10 mm between each step. Values of $d\mu_{ss} / d\ln V$ were measured by determining the local steady state friction μ_{ss} before and after the change in velocity (Figure 2). Trends in the absolute frictional level, on which are superimposed the velocity-dependent friction changes, are assumed to have no effect on the friction velocity dependence, a common assumption in studies of this type. Where significant ambiguity exists in the friction level before or after the step, a range of possible values was determined. Otherwise, the measurements of $d\mu_{ss} / d\ln V$ are considered correct to ± 0.001 .

The measured friction is the combination of rock friction and contributions from the jacket assembly consisting of Teflon rings, Viton O-rings, and the alignment bearing assembly (Figures 1 and A1). The jacket assembly sliding friction component increases the measured value of the coefficient of friction by about 0.01. For the purposes of the present study it suffices to neglect the absolute friction of the assembly. Jacket assembly friction has a positive velocity dependence which changes the apparent values of $d\mu_{ss} / d\ln V$. Calibration experiments on jacketed and unjacketed samples of both lubricated steel and initially bare granite have determined an approximate, maximum jacket assembly contribution to $d\mu_{ss} / d\ln V$ of +0.001. Values of $d\mu_{ss} / d\ln V$ reported here have been corrected for jacket assembly effects by subtracting 0.001.

Simulated gouge experiments have an additional contribution to the shear resistance from the Teflon rings beyond that present in bare experiments. Initially, the upper and lower Teflon jackets (Figure 1) are connected by a ~ 0.002 inch web of Teflon adjacent to the sample. This web keeps the gouge from extruding between the jacket halves during sample preparation and is absent in the bare experiments. Initially, the web introduces a shear resistance which decreases to zero over a few millimeters. The friction velocity dependence of an experiment with no web (FR107) shows no significant difference from those of experiments with the web. Since the contribution is small and affects only the first few velocity steps, no correction to the friction velocity dependence has been made.

Sample Displacement

Sample displacement is determined by a high-resolution resolver [Weeks and Tullis, 1992] whose body is mounted on the upper sample grip. The resolver's rotating shaft is attached to the lower sample grip via an elastic bellows (Figure 1) which is compliant in the axial direction but stiff in torsion. Displacement resolution of the resolver along the radial midline of the sample is $\sim 0.074 \mu\text{m}$.

Gouge Thickness

Changes in gouge thickness are determined from the relative length of the sample column. Column length is recorded by a linear variable differential transformer (LVDT) mounted to the upper sample grip whose core is attached to the lower sample grip (Figure 1). Changes in this length with displacement δ commonly accompany the imposed changes in sliding velocity which are used to determine the friction velocity dependence (Figure 3). We

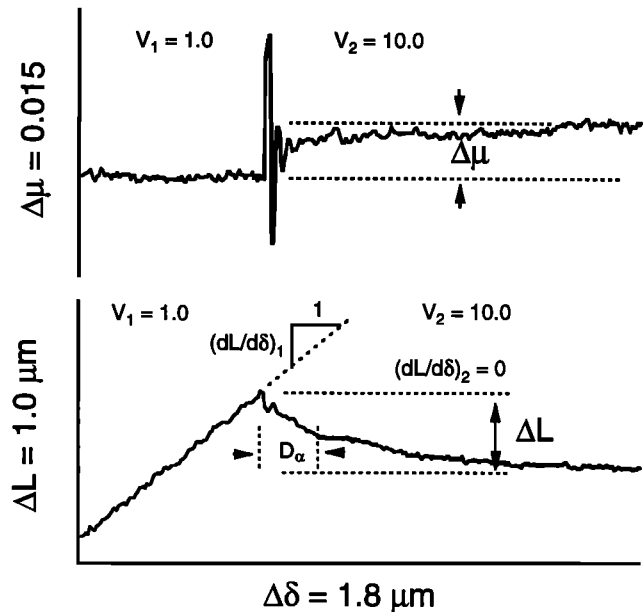


Figure 3. Typical response of frictional strength and gouge thickness to an increase in sliding velocity for simulated gouge at large displacement. (top) Friction. The compliance of the apparatus allows oscillations in friction and slip rate before a new steady state is reached. (bottom) Gouge thickness. In response to the change in sliding velocity there is both a change in dilation rate from $(dL/d\delta)_1$ to $(dL/d\delta)_2$ and an offset ΔL which has an apparent length scale D_α . In general, $(dL/d\delta)_2$ is nonzero, unlike this example.

interpret these length changes as inelastic changes in gouge thickness L because all other components of the sample assembly are elastic and the normal stress on the fault is constant. The resolution of the LVDT is $\sim 0.01 \mu\text{m}$.

Changes in gouge thickness L that accompany changes in sliding velocity can be described by two components: (1) a change in the steady state dilation rate, the change of L with respect to displacement δ , $(dL/d\delta)_{ss}$, namely, $\Delta(dL/d\delta)_{ss}$ [Marone *et al.*, 1990], and (2) a net offset in thickness ΔL which occurs over a characteristic displacement D_α [Marone and Kilgore, 1993] (Figure 3). The relative sizes of $\Delta(dL/d\delta)_{ss}$, ΔL , and D_α were determined using an empirical equation fit to the data following the velocity change:

$$L = L_0 + \Delta L \left\{ 1 - \exp\left[(\delta_0 - \delta) / D_\alpha \right] \right\} + \Delta(dL/d\delta)_{ss} (\delta - \delta_0) \quad (3)$$

where L_0 and δ_0 are constants equal to the values of L and δ at the velocity change. The exponential form is chosen primarily because the data follow a nearly exponential decay with displacement but also because the contribution to friction given by θ in equation (1) is exponential in displacement at constant velocity and previous work suggests a correlation between friction and layer thickness [Marone and Kilgore, 1993].

Results

Mechanical results and microstructures of long-displacement experiments on both initially bare surfaces and simulated gouge samples are described in the following four subsections. To simplify the description, "simulated gouge" and "initially bare" are referred to as "sample configurations." The approach used throughout the paper is to present the characteristic mechanical behavior using two "typical" experiments (FR121 and FR90), one

for each configuration. In cases where a range of behavior is observed, additional representative examples are shown. Friction, gouge thickness and friction velocity dependence data for all experiments are shown in Appendix B.

Friction

Systematic variations in friction with displacement are characteristic of each sample configuration. Slip on initially bare surfaces results in strengthening with displacement (Figure 4a). The rate of strengthening with displacement decreases with displacement but remains positive to 100 mm (Figure 4a). Subsequent slip results in little or no strength variation with displacement, μ being ~ 0.75 . Simulated gouges undergo both displacement strengthening and weakening (Figure 5a). At the outset, strength increases rapidly with displacement, reaching an initial peak strength of ~ 0.8 at 1–2 mm of slip. Subsequently, gouge undergoes protracted weakening, reaching a minimum strength of ~ 0.63 after 40 mm of slip. Among all simulated gouge experiments there is variation in the magnitude of the initial peak strength (0.74–0.80) and of the strength minimum (0.60–0.68). Following the minimum, renewed strengthening leads to a broad maximum of ~ 0.70 between 100 and 200 mm, followed by weakening to a fairly constant level of 0.67. The general pattern of peak strength, strength minimum, and restrengthening with displacement occurring within the first 150 mm is observed in all simulated gouge experiments.

Friction Velocity Dependence

The velocity dependence of friction in the early stages of initially bare surface experiments is not reproducible and can be either negative or positive. The lack of reproducibility in the initial friction velocity dependence is consistent with results reported elsewhere. Whereas other workers have “conditioned” samples by slip of many millimeters to many centimeters prior to measurement of the friction or friction velocity dependence [Dieterich, 1978; Linker and Dieterich, 1992], our experiments have undergone no prior displacement. Lack of reproducibility is assumed to result from differences in initial surface roughness and contact area [see Biegel *et al.*, 1992]. With displacement, the friction velocity dependence, whether initially negative or positive, converges to velocity weakening after no more than 15 mm slip, attaining an average value of -0.0031 (Figure 4b).

Simulated gouge exhibits velocity strengthening at short displacement (Figure 5b) and evolves with slip to velocity weakening ($d\mu_{ss} / d\ln V$ in the range $+0.0000$ to -0.0010) by 40 mm. This velocity strengthening followed by velocity weakening is reproducible. The transition to velocity weakening does not occur until the sample has slid more than 18 mm. With displacement beyond 50 mm, the friction velocity dependence increases to velocity strengthening/neutral and remains so to 400 mm displacement (Figure 5b). There is a large variation between experiments in the magnitude of the friction velocity dependence at large displacement (100–400 mm). The example experiment shown (Figure 5) has the smallest friction velocity dependence of the five simulated gouge experiments, with $d\mu_{ss} / d\ln V \sim +0.0005$. The experiment with the highest average friction velocity dependence at large displacement yields $\sim +0.004$ (see Figures B2 and 6a for comparison with Figure 5b).

Gouge Thickness

Gouge thickness changes for both sample configurations show an overall trend of compaction with displacement, but the details

of thickness changes depend on sample configuration. For initially bare surfaces the sample compacts rapidly (Figure 4c), accomplishing 30 μm of shortening within the first 20 mm of displacement. Further slip causes continued thinning at a considerably reduced rate (Figure 4c); the rate of compaction with displacement decreases with displacement out to 40 mm. A small portion of this response may be due to a small amount of gouge being extruded from between the granite surfaces. Subsequent displacement results in no compaction and slight dilation between 40 and 120 mm displacement. At larger displacements the details of compaction versus displacement differ for each initially bare surface experiment (Figure B1), but on average, all show continued compaction with displacement.

Simulated granite gouge initially undergoes a similar, but larger, reduction in thickness (Figure 5c) as compared with initially bare surfaces, and it continues out to nearly 50 mm. The fault compacts by 50 μm over the first 50 mm displacement. After the initial rapid compaction the rate of compaction with displacement is generally quite small, and the gouge is often observed to dilate very slightly over the displacement range of 40–120 mm. At larger displacements the overall trend shows continued compaction although transient dilation is observed.

Velocity Dependence of Gouge Thickness

Both initially bare surfaces and simulated gouges show measurable changes in thickness following changes in sliding velocity (insets in Figures 4c and 5c) which are superimposed on the overall trends in compaction with displacement. Increases in velocity lead to sample dilation and decreases lead to sample compaction. Following a velocity change there can be both immediate and steady state changes in dilation rate ($dL / d\delta$). Figure 5c at 2.6 mm displacement shows a clear example. When the velocity decreases there is an instantaneous increase in the compaction rate (inset c1). With continued slip the gouge continues to compact at a rate which decreases with displacement. After $\sim 200 \mu\text{m}$ the rate has ceased to decrease appreciably, establishing an approximately constant rate of compaction which is higher than the rate prior to the change in velocity. The response to an increase in velocity is similar but is of the opposite sense to a decrease. There is an immediate decrease in the compaction rate, following which the rate gradually approaches a new steady state compaction rate which is smaller than that prior to the change in velocity (Figure 3).

Both the change in the steady state compaction rate and the amount of immediate change in thickness are smaller for initially bare surfaces than those observed in simulated gouges. This can be seen by comparing the vertical scales on insets accompanying Figures 4c and 5c. The size and form of thickness changes with changes in sliding velocity reach a “steady state” response for bare surfaces after 20 mm displacement (compare Figure 4c, insets c2–c4).

For simulated gouges the thickness changes accompanying changes in sliding velocity depend on the total displacement. At short and long displacements, changes in thickness accompanying changes in sliding velocity are large (Figure 5c, insets c1 and c3), corresponding to the region of velocity strengthening at small displacements and the region of velocity strengthening to velocity neutral behavior at large displacements. In some cases the dilation resulting from a velocity increase is large enough to overcome the overall compaction trend and results in an absolute dilation (Figure 3); in other cases it is not large enough to cause net dilation. At intermediate displacements, in the 20–50 mm interval

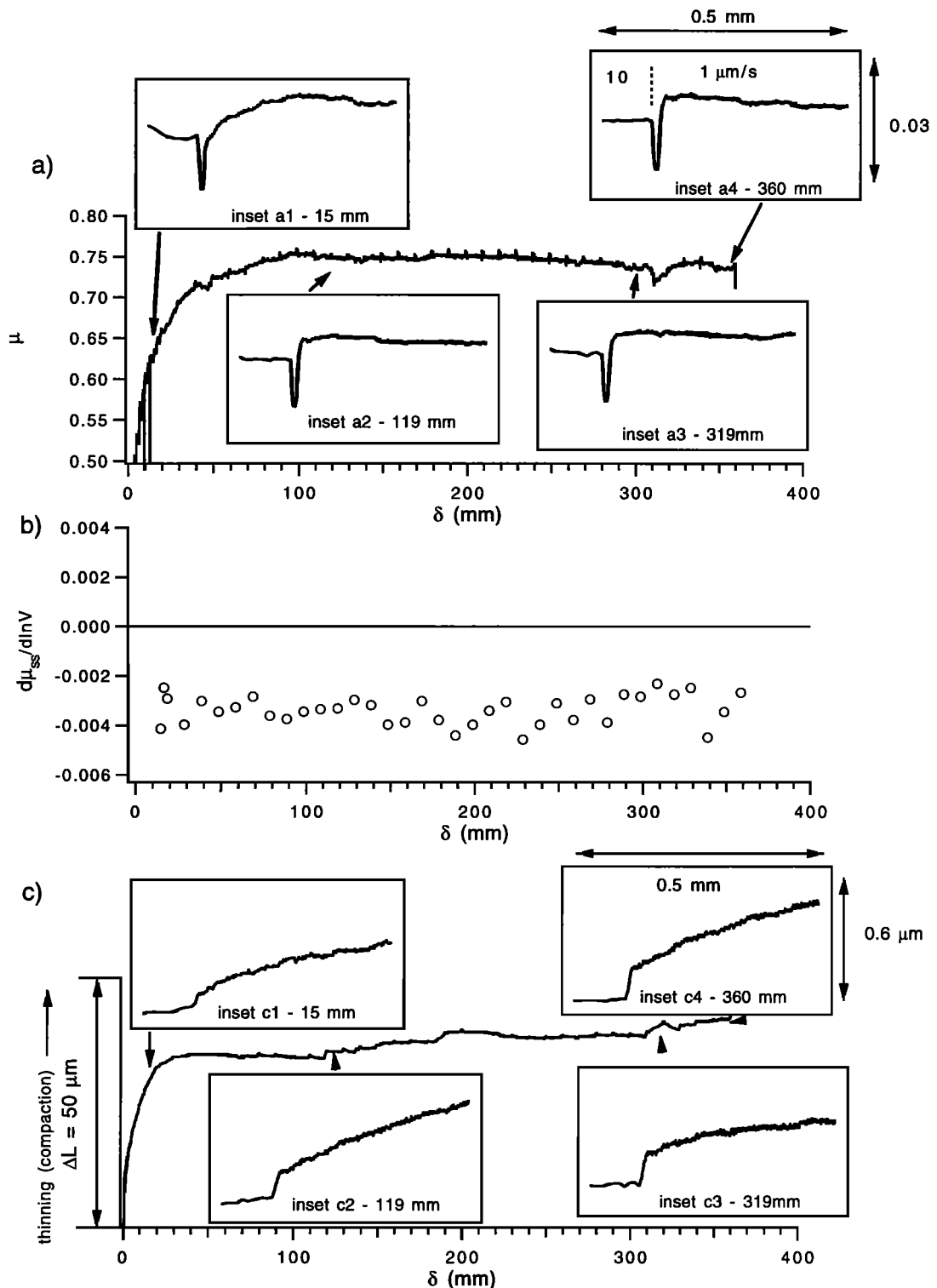


Figure 4. Summary of mechanical observations for a typical initially bare surface experiment (FR121). Data are averaged over $100 \mu\text{m}$ displacement. (a) Friction versus displacement. Large reductions in strength at 9 and 12 mm correspond to intentional unloading and reloading of the shear stress and are present for all experiments. For initially bare surfaces the unload/reload cycle has little or no effect on the strength. Most of the abrupt variations in friction visible are responses to changes in velocity. Insets show the details of the response to decreases in sliding velocity at four different displacements, all at the same scale. Horizontal and vertical scales for insets indicate the length of the arrows. (b) Friction velocity dependence versus displacement. (c) Changes in sample column length versus displacement. Changes in L are attributed to strain within the fault zone, normal to the fault plane. Insets show the details of the response of L to decreases in sliding velocity at the four different displacements, all at the same displacement scale shown in Figure 4a.

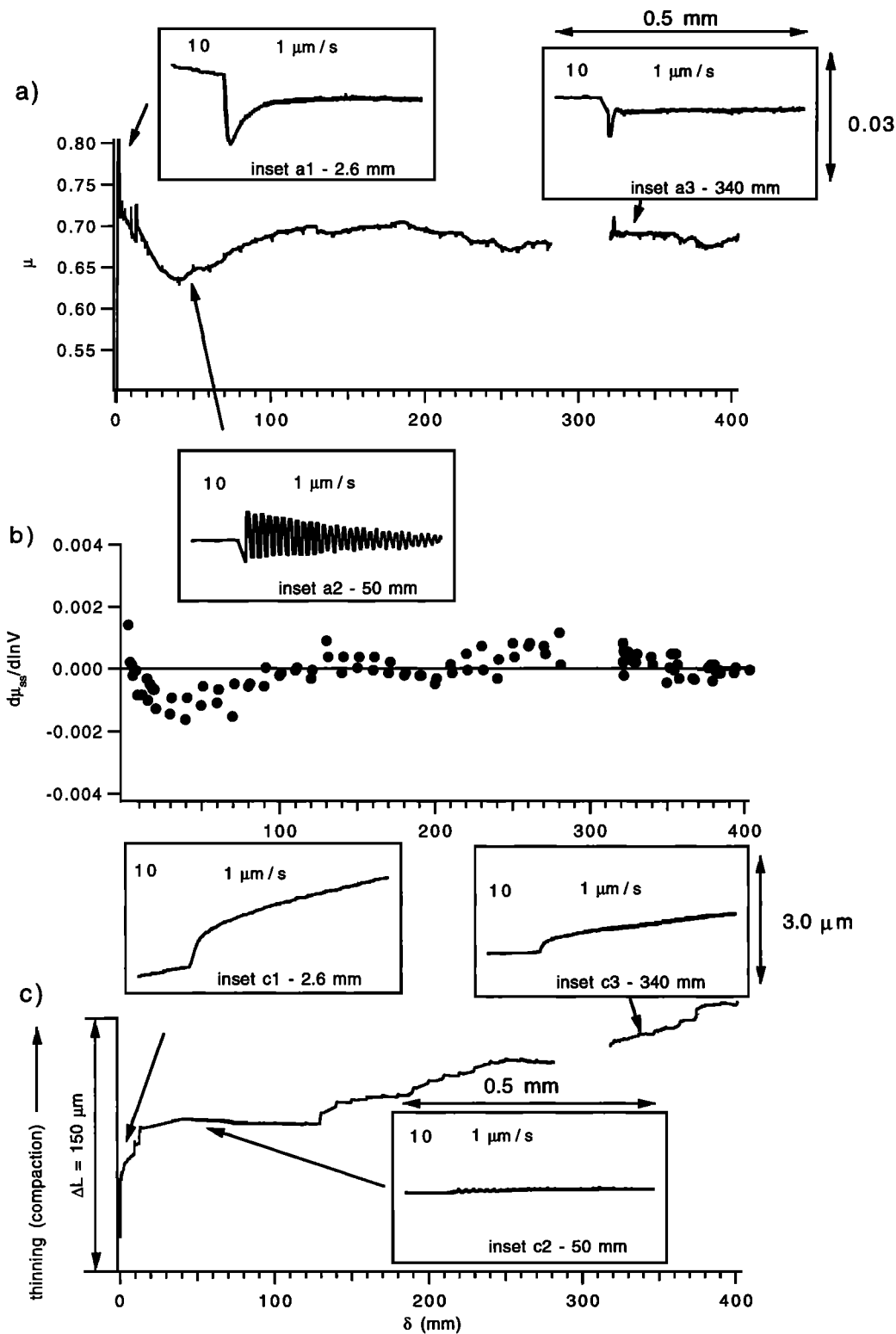


Figure 5. Summary of mechanical observations for a typical simulated gouge experiment (FR90). Figures 5a, 5b, and 5c correspond to Figures 4a, 4b, and 4c. Data are averaged over 100 μm displacement. The data gap from 282 to 320 mm corresponds to a technical problem with the confining pressure servo. Confining pressure dropped by less than 1% during this interval and the subsequent measurements were not adversely affected. In Figure 5a, intentional unloading and reloading of the shear stress occur at 9 and 12 mm in all simulated gouge experiments. These features are not always visible due to the averaging. Unload/reload cycles affect the strength of simulated gouges; the size of this effect varies between experiments, but in general strength increases follow the unload/reload cycle, as can be seen by the large spikes and the small offsets in μ at 9 and 12 mm. Horizontal and vertical scales for insets indicate the length of the arrows. In Figure 5c, the unload/reload cycles at 9 and 12 mm can lead to net compaction which is related to strengthening following the reload; see Figure 5a.

of slip when the sample strength is lowest and the friction velocity dependence is the most negative, changes in dilation rate are systematically smaller (Figure 5c, inset c2), similar to the initially bare surface response (Figure 4c).

These observations can be quantified by determining the net thickness changes described by $\alpha = \Delta L / \Delta \ln V$ [Marone and Kilgore, 1993] and the changes in dilation rate $\Delta(dL / d\delta)_{ss} / \Delta \ln V$

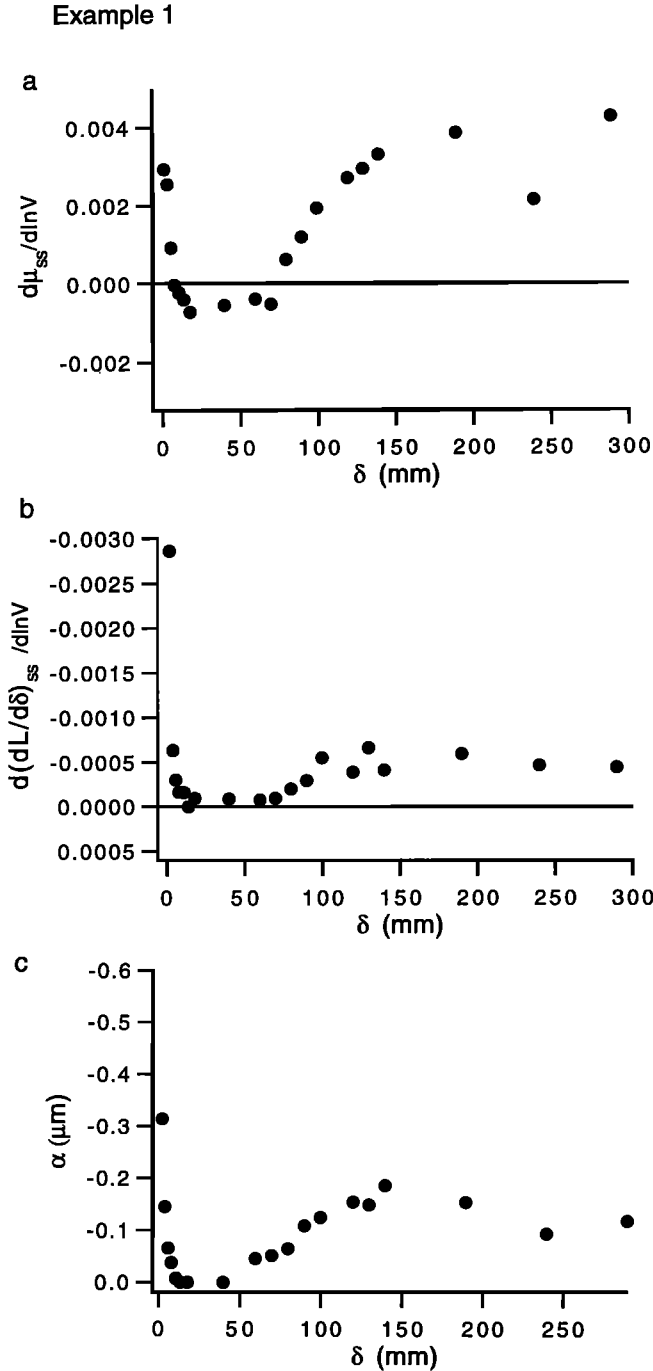


Figure 6. Correlation between steady state friction velocity dependence and dilation with displacement. Results from two experiments on simulated gouge are shown which indicate the range of results. For example 2 the results for velocity step increases and decreases are shown for comparison. For example 1, only step increases are shown. (a) Observed friction velocity dependence. (b) Velocity dependence of dilation rate. (c) Velocity dependence of the offset in L .

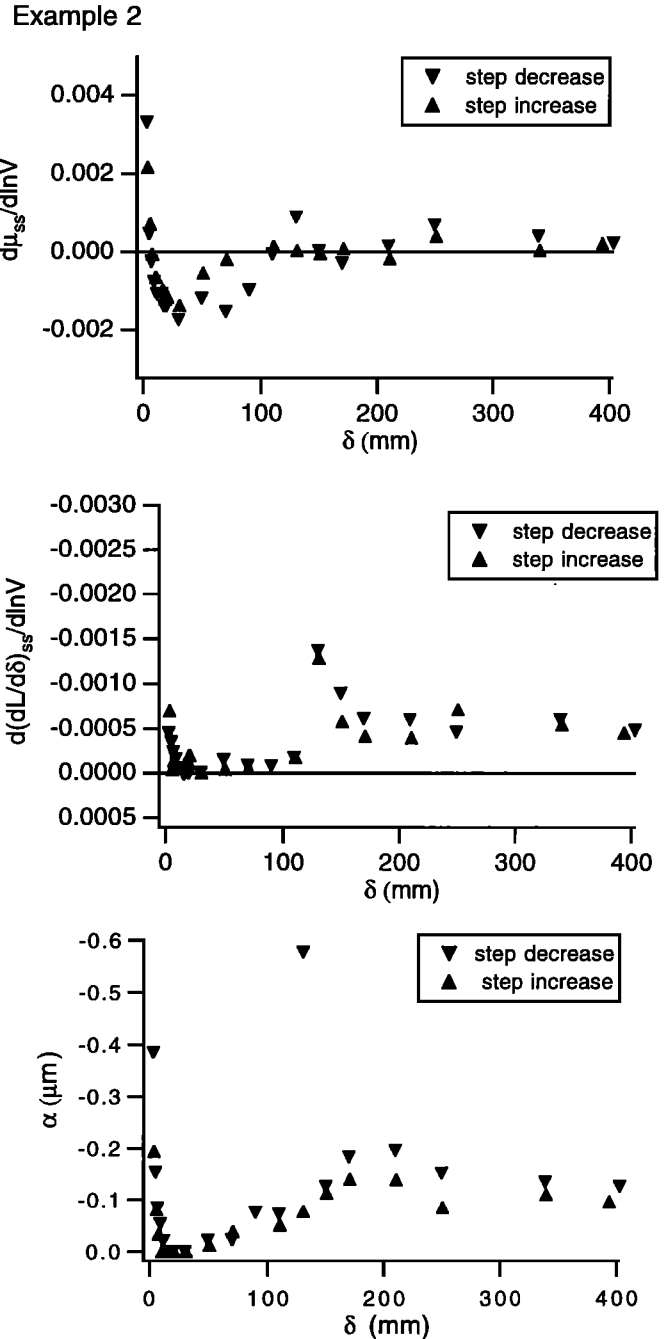


Figure 6. (continued)

[Marone et al., 1990] and comparing the results with the friction velocity dependence. Compaction and left-lateral shear strain are considered positive; therefore $dL / d\delta < 0$ indicates thickening with displacement. For a decrease in slip rate we observe compaction ($\Delta L > 0$) and an increase in the rate of compaction ($\Delta(dL / d\delta)_{ss} > 0$). For an increase in slip rate we observe dilation ($\Delta L < 0$) and a decrease in the rate of compaction with slip $\Delta(dL / d\delta)_{ss} < 0$. Therefore $\alpha < 0$ and $\Delta(dL / d\delta)_{ss} / \Delta \ln V < 0$. Both α and $\Delta(dL / d\delta)_{ss} / \Delta \ln V$ correlate with the friction velocity dependence at all displacements (Figure 6). Marone et al. [1990] first observed that $\Delta(dL / d\delta)_{ss} / \Delta \ln V$ was negative, but the correlation between α and $\Delta(dL / d\delta)_{ss} / \Delta \ln V$ and friction velocity dependence with displacement were not seen by Marone et al. [1990] because there is no displacement dependence of friction velocity depen-

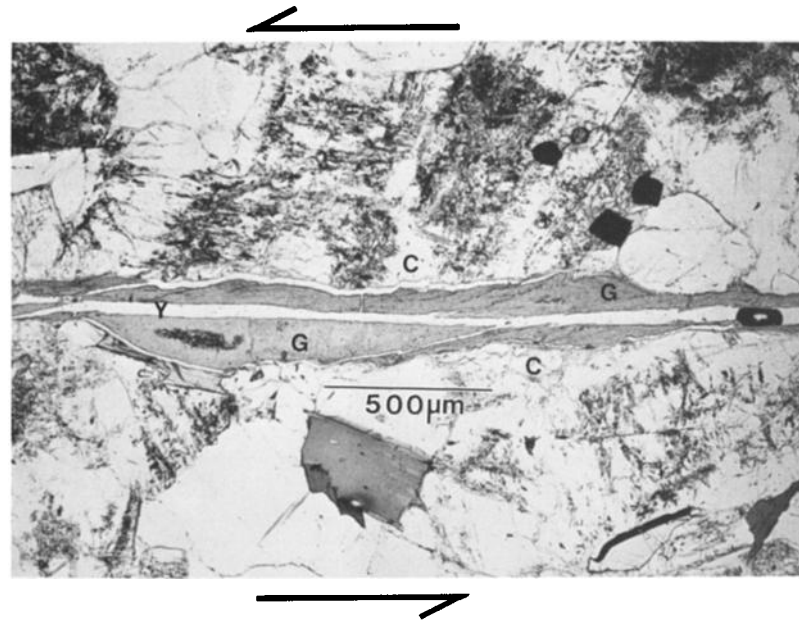


Figure 7. Optical photomicrograph of a mature fault zone generated from slip between initially bare surfaces of Westerly granite (C). At 375 mm slip (FR37), deformation is localized on a flat Y shear (Y). Gouge (G) is fine-grained throughout. During unloading, the gouge layer has separated along the Y shear and at the gouge-rock interfaces.

dence in their shorter displacement experiments. A similar correlation between α and friction velocity dependence was noted by Marone [1993], who observed a displacement dependence of friction velocity dependence. Marone and Kilgore [1993] have suggested that α reflects a change in thickness of the actively deforming layer so that large values of α reflect a thick deforming layer.

Microstructures

For the thin gouge layers produced in initially bare surface experiments, shearing results in a microstructure which is dominated by boundary-parallel Y shears [Logan *et al.*, 1979] (Figure 7). R_1 shears are prominent during the early stages of deformation (< 18 mm) but give way to Y shears with continued deformation (M. L. Blanpied, unpublished data, 1989). At large displacements, remnant R_1 shears can be identified in the gouge to either side of a Y shear; these are never observed to offset a Y shear. The geometry of the Y shear appears to be unaffected by irregularities in the gouge-rock interface or by local variations in gouge thickness, suggesting that little or no bulk simple shear occurs in this "mature" microstructural state. Thus displacement appears to be accommodated almost entirely on the Y shears.

Experiments on layers of simulated gouge show a more complex evolution of gouge microstructure. At short displacements (10 mm) (Figure 8a), the bulk of the gouge appears identical to undeformed (<90 μm) gouge, with a wide distribution of particle sizes. Shear is concentrated in a finite band near the lower gouge-rock interface, as indicated by a reduction in the number of large particles. Deformation in all simulated gouges occurs initially near the lower, not the upper, gouge-rock interface (see discussion section).

At intermediate displacements (~65 mm) (Figure 8b), the particle size has been greatly reduced in a narrow band near the lower boundary of the gouge but has remained large elsewhere in the gouge. The narrow band, when examined at high magnifica-

tion, appears foliated, with the foliation defined by many anastomosing semiparallel surfaces. These Y shears are, in general, darker in color than the surrounding gouge and contain no particles visible at the optical scale.

With displacements to 407 mm (Figure 8c), the fine-grained, foliated band expands upward into the less deformed gouge, and the upper portions of the gouge show evidence of distributed deformation. In the lower 250 μm of the gouge there is a complex network of Y shears (Figure 8c). This network contains many distinct boundary-parallel Y shears, plus numerous other shears which crosscut the gouge at low angles. R_1 shears can be seen in the approximately homogeneous, fine gouge in the lower central portion of the layer, above but not cutting the Y shears. In the upper half of the gouge layer the average particle size is considerably reduced from that seen at intermediate displacements, and evidence for distributed deformation can be seen in the presence of oriented biotite grains. These grains form an inclined planar fabric, suggesting the orientation of a strain ellipse for bulk simple shear. It appears that gouge near the upper boundary of the lower, highly foliated band becomes finely comminuted with development of the R_1 shears; the foliated band then widens when a Y shear forms in this fine-grained gouge.

Discussion

An important result of this study is the correlation between the friction velocity dependence measurements and the fault zone microstructures in either fault configuration. When deformation is localized in a single narrow shear band, where deformation occurs predominantly on Y shears, the friction velocity dependence is negative. This includes initially bare surfaces after a few millimeters of slip and simulated gouge experiments in the displacement range of 30-65 mm. Furthermore, in situations where the deformation is distributed, where we take distributed to mean as in bulk simple shear and also when wide or multiple shear

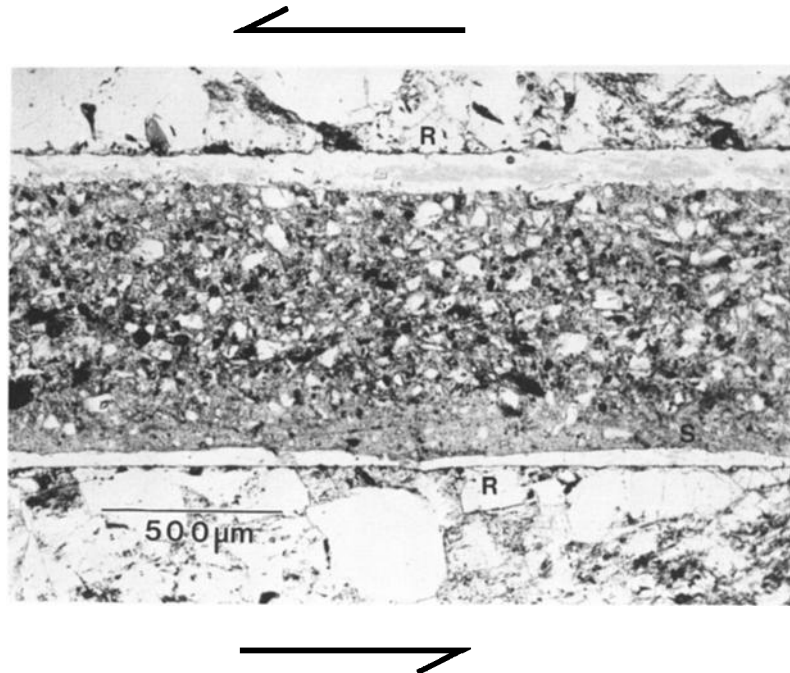


Figure 8a. Optical photomicrograph of simulated granite gouge (G) sheared to 10 mm displacement (FR57). Only gouge is shown (adjacent rocks (R) were not the sample forcing blocks). Grain size is reduced in an incipient shear zone (S) in the 100 μm nearest the lower interface.

zones are present, the friction velocity dependence is more positive (velocity strengthening/velocity neutral). This is seen in the simulated gouge microstructures at very short displacements and at displacements >70 mm. The correlation between friction velocity dependence and the degree of localization leads to two separate questions which are the focus of the following discussion: First, at any displacement, what controls the degree of local-

ization in each sample configuration? Second, why is distributed deformation more positively velocity dependent than localized deformation?

What Controls the Degree of Localization?

For initially bare surfaces the degree of localization is fixed: deformation is required to be localized because the actively de-

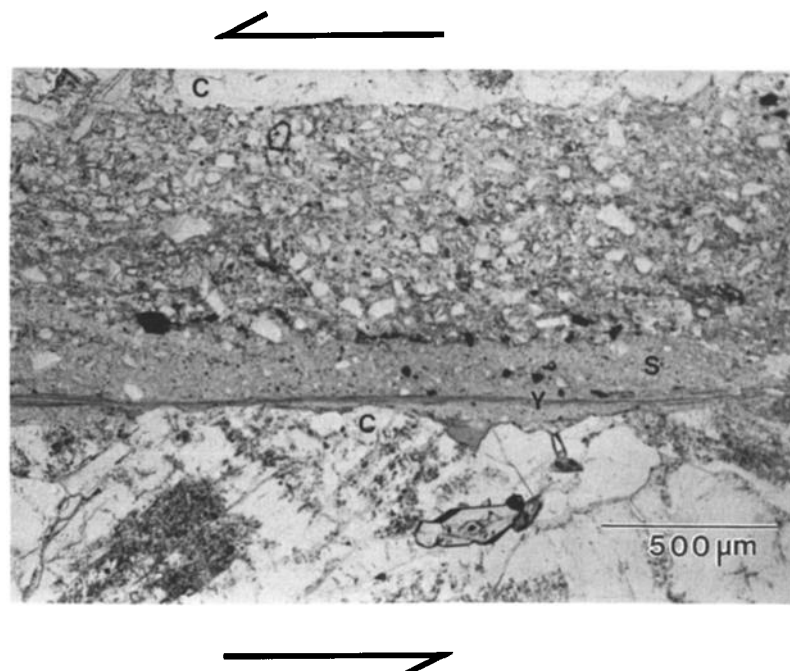


Figure 8b. Optical photomicrograph of simulated granite gouge (G) sheared to 65 mm displacement (FR66). The forcing blocks are labeled (C). Within the shear zone (S), a dark band of extremely fine-grained material has formed near the rock interface which contains a dominant boundary-parallel Y shear (Y).

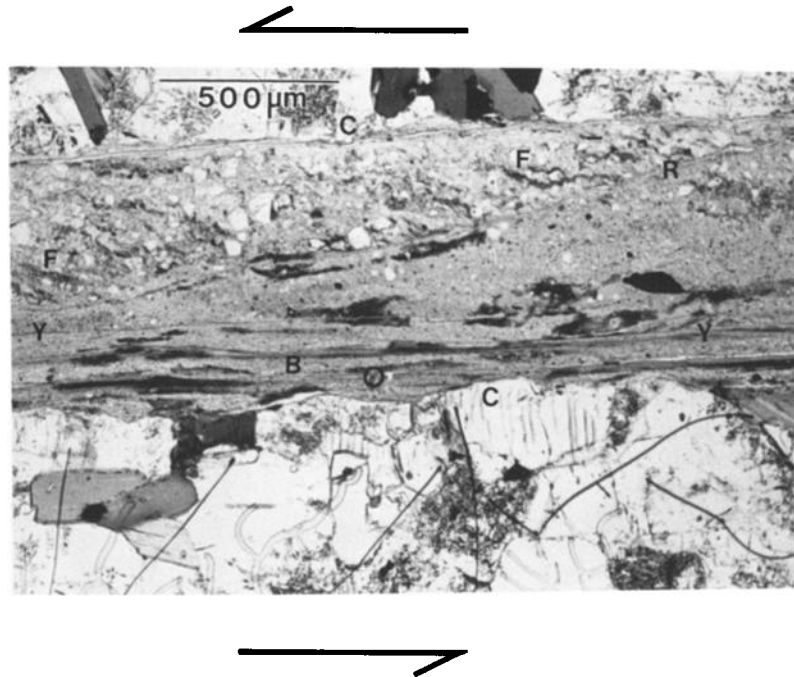


Figure 8c. Optical photomicrograph of simulated granite gouge (G) sheared to 407 mm displacement (FR60). A thick, foliated, fine-grained band (B), contains multiple Y shears. Directly above the foliated band is a homogeneous zone and above that is a less deformed zone with R_1 shears (R) as well as a foliation (F) defined by aligned biotite grains.

forming region is always weaker than its surroundings. This can be understood in the following way. In initially bare experiments a small amount of gouge is produced during slip by the breaking and crushing of highly stressed asperities at the outset of the experiment. *Power et al.* [1988] measured the increase in gouge thickness with displacement and showed that gouge is produced until it is of sufficient thickness to prevent contact of the opposing rough rock surfaces. The subsequent rate of gouge production goes nearly to zero, and all further deformation occurs within a gouge layer of approximately constant thickness. For the surface roughness used in our initially bare surface experiments, this limiting thickness is established within 18 mm of slip (the shortest displacement for which we have made optical observations); the average limiting thickness is 70–112 μm . Although the gouge layer has a finite total thickness, the majority of the total thickness of the gouge zone fills the roughness of the rock surfaces and undergoes little shear. The effective thickness of the gouge zone, the thickness between planes tangent to the asperities on opposing sides of the fault, is approximately zero [Beeler and Tullis, 1995]. This extremely thin effective layer will continue to accommodate the majority of the deformation so long as its shear failure strength remains lower than the surrounding rock. Previous studies indicate that the strength of intact rock exceeds the friction of ground or natural joint surfaces [e.g., Lockner and Byerlee, 1993]; thus the deformation of initially bare surfaces is constrained by the fault zone strength relative to the surroundings to remain localized.

For simulated gouges the deformation is not required to be localized. At any instant, if the actively deforming region is not the entire thickness of gouge and if the strength of the actively deforming region changes with time or displacement, then the location of deformation and also the degree of localization can change. In fact, in the first 100 mm of displacement in a simu-

lated gouge experiment there are large changes in strength with displacement, and the microstructural observations demonstrate that these changes in strength are accompanied by changes in the location of the deformation and in the degree of localization. These observations suggest that the degree of localization at any displacement is liable to be related to the displacement dependence of strength.

How strength and the degree of localization as a function of displacement are related in these gouge experiments can be better understood by considering a generalized fault whose shear strength τ is a function of strain (displacement dependent) and also of strain rate (velocity dependent), $\tau = f(\gamma, \dot{\gamma})$. In such a fault zone the rate of strength change with the change in thickness h_d of the deforming zone is

$$d\tau = -\frac{1}{h_d^2} \left(v \frac{\partial \tau}{\partial \dot{\gamma}} + \delta \frac{\partial \tau}{\partial \gamma} \right) dh_d, \quad (4)$$

where h_d is not necessarily the entire thickness of the fault zone h_f , engineering strain $\gamma = \delta / h_d$, $\dot{\gamma}$ is engineering strain rate, $\partial \tau / \partial \dot{\gamma}$ is the strain rate dependence of strength and $\partial \tau / \partial \gamma$ is the strain dependence of strength. Equation (4) provides a relationship between fault zone thickness change and increment of strength change.

As required by energy considerations, the strength of a fault tends to be minimized, provided there is a path by which weakening can occur. Thus $d\tau$ is negative, and as a result, the fault can become weaker either by localizing ($dh_d < 0$) or becoming less localized ($dh_d > 0$). For instance, if there is no velocity dependence of strength ($\partial \tau / \partial \dot{\gamma} = 0$) and the displacement dependence of strength is negative, then to minimize strength, $d\tau / dh_d$ must be negative, requiring that the fault will localize (dh_d is negative). Conversely, if there is no velocity dependence of strength

($\partial\tau / \partial\dot{\gamma} = 0$) and the displacement dependence of strength is positive, to minimize strength requires that the fault will delocalize (dh_d is positive).

In the case of simulated gouge the velocity dependence and the displacement dependence are both nonzero. Therefore, whether the fault localizes or not depends on which term on the right-hand side of (4), the displacement dependence or the velocity dependence, is larger. Equation (4) cannot be used with measurements of the displacement dependence of friction and friction velocity dependence to predict changes in the degree of localization because the terms in (4) are partial derivatives and the measurements have not been made independently. However, the friction velocity dependence and friction measurements can be used with microstructural observations to infer which term on the right-hand side of (4) is larger. For example, textural evidence suggests that localization begins between 0 and 10 mm displacement when the friction velocity dependence is positive. In the absence of displacement dependence, positive friction velocity dependence should lead to delocalization. Therefore the observed localization is likely to have resulted from friction displacement dependence, not the friction velocity dependence. Similar arguments can be applied to the delocalization. In the neighborhood of the strength minimum the friction velocity dependence is negative, a condition which, if acting alone, would result in localization. Instead, delocalization is observed which must therefore result from the displacement dependence of fault zone strength. In both examined cases, the displacement dependence is apparently the independent variable which controls the degree of localization and leads to changes in the friction velocity dependence.

Although the experiments provide no quantitative data on what factors control the displacement dependence of strength during either displacement weakening or strengthening, some plausible explanations can be offered. The weakening between 2 and 40 mm is apparently due to the production of a Y surface along the lower gouge-rock interface. This surface perhaps has less sliding resistance because it is essentially planar and so resistance due to interlocking particles and asperities is minimized. The lower gouge-rock interface is favored for localization over the upper because the splits in the Teflon jackets are closer to the lower interface (see Appendix A), the split in the jacket provides a localized boundary condition that encourages localized slip to propagate into the gouge somewhat like a mode III crack. A plausible explanation for the subsequent strengthening is that continued comminution fills in previous voids along this Y surface, resulting in a higher real area of contact, and increasing frictional resistance. The behavior is similar to that observed by Mandl *et al.* [1977, pp. 112-119] whose experimentally produced shear zones in granular aggregates widened with displacement, and by Aydin [1978] and Aydin and Johnson [1978] whose natural shear zones in porous sandstones widened as they densified.

Why Is the Friction Velocity Dependence of Distributed Deformation More Positive Than That of Localized Deformation?

Role of dilatancy. Observations that the friction velocity dependence during distributed deformation in simulated gouge is more positive than that observed during localized slip in gouges or bare surfaces have been made in many previous short displacement experiments [Summers and Byerlee, 1976; Solberg and Byerlee, 1984; Lockner *et al.*, 1986; Morrow and Byerlee, 1989; Biegel *et al.*, 1989]. Of the existing explanations for this observation only that of Marone *et al.* [1990] has a theoretical

basis and is supported by experimental measurements. Marone *et al.* [1990] hypothesized that the friction velocity dependence of simulated gouge is the sum of the friction velocity dependence of bare surfaces and the velocity dependence of dilation rate. This explanation is appealing for the experiments in this study because, as we have already shown, the friction velocity dependence and $\Delta(dL/d\delta)_s / \Delta \ln V$ correlate at all displacements. In the following discussion, we rederive and test Marone *et al.*'s [1990] hypothesis that dilatancy of gouge explains the increase in friction velocity dependence.

The theoretical basis for this hypothesis is a relationship between stress and strain within the gouge layer derived by determining all of the work done on the deforming body by the external tractions and equating it to all of the energy dissipated or stored during the deformation. The work per unit volume done by external surface tractions ($dW = \sigma_{ij} d\epsilon_{ij}$) on a body deforming along a fault zone with planar boundaries, ignoring contributions from emitted acoustic energy, is equal to the energy dissipated within the fault zone ($dQ = \tau^f d\gamma$), neglecting energy stored as surface area. Thus

$$\tau^f d\gamma = \sigma_{ij} d\epsilon_{ij}, \quad (5)$$

where σ_{ij} is the stress tensor, $d\epsilon_{ij}$ is the incremental strain tensor, τ^f is the frictional resistance, and $d\gamma$ is the shear strain of the fault zone.

When evaluated for measured shear resistance, (5) generally does not lead to the same expression for bare surfaces and simulated gouges, as is shown next. First, consider a bare surface fault where all of the strain occurs as shear strain parallel to the fault boundaries. In this case, $dW = \sigma_{ij} d\epsilon_{ij} = \tau^A d\gamma$, where τ^A is the applied shear stress, and so from (5) we find that $\tau^A = \tau^f$ as could be deduced from stress equilibrium. For a finite-width zone such as simulated gouges, recent studies have shown that fault thickness is a function of displacement and that thickness also changes in response to changes in sliding velocity [Morrow and Byerlee, 1989; Marone *et al.*, 1990; Marone and Kilgore, 1993; Scott *et al.*, 1994]. Thus, for gouge, $\sigma_{ij} d\epsilon_{ij}$ does not necessarily reduce to a single term. In some cases the change in thickness makes a considerable contribution to the resistance to deformation [Scott *et al.*, 1994] and/or to the velocity dependence of the resistance [Marone *et al.*, 1990]. In these cases, if there is no length change in the plane of the fault, then $dW = \tau^A d\gamma + \sigma_n d\epsilon_n$, where σ_n and ϵ_n are the stress and strain normal to the fault boundary. Thus frictional resistance τ^f is not equal to the applied shear stress, because

$$\tau^f d\gamma = \tau^A d\gamma + \sigma_n d\epsilon_n$$

so

$$\mu^A = \mu^f - d\epsilon_n / d\gamma, \quad (6)$$

where $\mu^f = \tau^f / \sigma_n$ and $\mu^A = \tau^A / \sigma_n$ is the apparent friction coefficient [Edmond and Paterson, 1972]. Noting that $d\epsilon_n = dL / L_0$ and $d\gamma = d\delta / L_0$ [e.g., Mandl *et al.*, 1977], (6) becomes

$$\mu^A = \mu^f - dL / d\delta. \quad (7)$$

For compaction, dL is positive as is all work done on the deforming material. Equation (7) is equivalent to equation (7) of Marone *et al.* [1990]. We refer to μ^f as the intrinsic friction coefficient, as defined by (6) or (7), the friction coefficient in the absence of dilatancy. In soil mechanics, where (6) was first used [e.g., Bishop, 1959], μ^f is a material property.

The desired relationship between the observed steady state friction velocity dependence and the velocity dependence of dila-

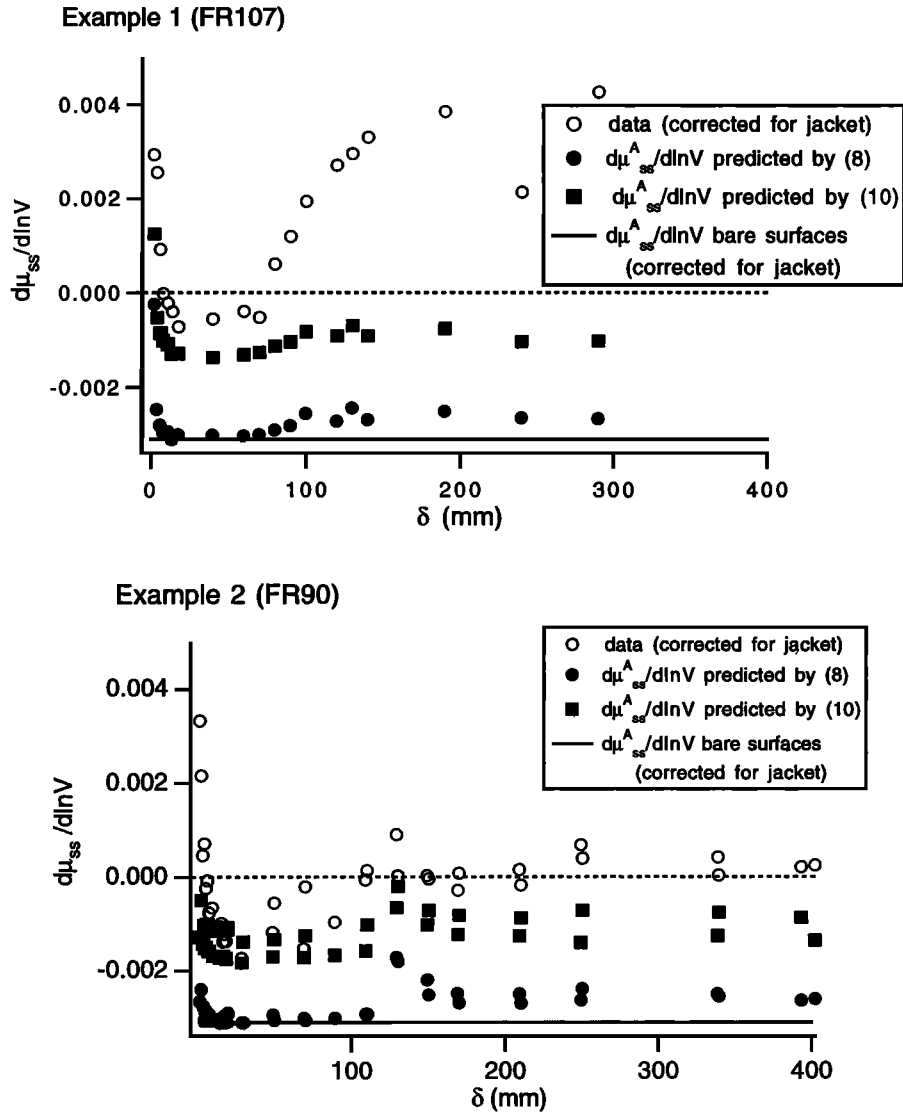


Figure 9. Comparison between data and predictions of the velocity dependence of friction for simulated gouge. The predictions are based on the contribution of the velocity dependence of dilation rate from equations (8) and (10), assuming that the intrinsic friction velocity dependence equals that measured in initially bare surface experiments.

tion rate is obtained by taking the derivative of (7) with respect to $\ln V$ and applying it to the steady state condition:

$$\frac{d\mu_{ss}^A}{d\ln V} = \frac{d\mu_{ss}^I}{d\ln V} - \frac{d(dL/d\delta)_{ss}}{d\ln V}, \quad (8)$$

where we refer to $d\mu_{ss}^A/d\ln V$ as the observed or apparent friction velocity dependence, $d\mu_{ss}^I/d\ln V$ as the intrinsic friction velocity dependence, and $d(dL/d\delta)_{ss}/d\ln V$ as the velocity dependence of dilation rate.

The hypothesis of Marone *et al.* [1990] is that $d\mu_{ss}^I/d\ln V$ of simulated gouge is identical to the measured friction velocity dependence of bare surfaces; thus according to (8), $d\mu_{ss}^A/d\ln V$ of simulated gouge is the sum of the measured velocity dependence of dilation rate and the friction velocity dependence of bare surfaces. To test this hypothesis, we have used the friction velocity dependence of bare granite surfaces (roughly -0.0031) and measured values of $d(dL/d\delta)_{ss}/d\ln V$ (Figure 6b) to calculate the predicted value of $d\mu_{ss}^A/d\ln V$ as a function of displacement (Figure 9, solid circles). At no displacement is the predicted value

of $d\mu_{ss}^A/d\ln V$ large enough to explain the observed friction velocity dependence (open circles). This result suggests that the intrinsic friction velocity dependence of simulated gouge is more positive at all displacements than the friction velocity dependence of initially bare surfaces and that intrinsic friction velocity dependence changes with displacement. Both these results apparently contradict the results of Marone *et al.* [1990]. That $d\mu_{ss}^I/d\ln V$ varies with displacement suggests that as defined, μ^I is not an intrinsic property of the material.

Implicit in (8) is the assumption that frictional dissipation occurs parallel to the fault boundaries; as we consider next, theoretical and experimental results suggest this may not be true for simulated gouges. In the case where frictional dissipation occurs on surfaces inclined to the fault boundaries, the predicted contribution of the velocity dependence of dilatancy to measured friction velocity dependence in (8) may be in error. Textural observations from both natural and experimental gouge layers suggest that deformation is accommodated at short displacements by deformation on R_1 planes which are typically oriented $\sim 15^\circ$ from

the fault boundaries [Logan *et al.*, 1979; Morrow and Byerlee, 1989; Biegel *et al.*, 1989; Marone *et al.*, 1990; Marone and Kilgore, 1993; Blanpied *et al.*, 1995]. The R_1 planes have been interpreted as Mohr-Coulomb failure planes, in which case, if the gouge is mechanically isotropic, the greatest compressive stress σ_1 within the fault zone is oriented at 45° from the fault boundary [Hobbs *et al.*, 1990; Marone *et al.*, 1992; Byerlee and Savage, 1992], and overall simple shear of the gouge is accomplished by cooperative slip on sets of conjugate R_1 and R_2 planes. Mandl *et al.* [1977] observed this special 45° orientation of stress during shear by embedding devices which measure the stress orientation in the gouge layer. If cohesion is ignored, the measured friction μ^A is specified by the true friction μ^T on the deforming planes and the angular relation between the true and apparent planes is

$$\mu^A = \sin(\tan^{-1} \mu^T). \quad (9)$$

[Hobbs *et al.*, 1990; Marone *et al.*, 1992; Byerlee and Savage, 1992]. In the following discussion we use the superscript T to denote true as seen by an observer on the deforming R_1 or R_2 planes and superscript A to denote apparent as seen in the measurement plane.

If gouge actually deforms on inclined planes such as represented by (9), the observed friction velocity dependence (8) must be modified to reflect the true geometry of the deformation. For the case of macroscopic simple shear ($d\epsilon_n^A / d\gamma^A = 0$), the apparent friction velocity dependence is smaller in magnitude than the true friction velocity dependence, and the difference between true and apparent friction velocity dependence varies with true friction [Beeler and Tullis, 1995]. In the current case, we wish also to consider how the contribution from the velocity dependence of dilatancy is related to the measured friction velocity dependence. Assuming that there is no in-plane normal strain, the resulting relationship is

$$\frac{d\mu_{ss}^A}{d \ln V} = -(\sin^4 \phi + \cos^3 \phi) \frac{d(d\epsilon_n^A / d\gamma^A)_{ss}}{d \ln V} + \cos^3 \phi \frac{d\mu_{ss}^T}{d \ln V}, \quad (10)$$

where ϕ is the friction angle and all other symbols have the same definition as in (8) [Beeler, 1995]. As was noted earlier, $d\epsilon_n^A / d\gamma^A = dL / d\delta$. Observed values for μ_{ss}^A and $dL / d\delta$ are used in equation (A2) from Beeler [1995] to determine ϕ . Using ϕ , measured values of $d(dL / d\delta)_{ss} / d \ln V$, and a bare surface value for $d\mu_{ss}^T / d \ln V$ (-0.0031), the predicted apparent friction velocity dependence from (10) is plotted as solid squares in Figure 9.

There is still a large discrepancy between the predictions of (10) and the observed friction velocity dependence data, although the discrepancy is considerably smaller than that predicted by (8). As did (8), (10) suggests that the intrinsic friction velocity dependence of these granite gouges is greater than that observed for bare surfaces, contradicting the results of Marone *et al.* [1990], and that the intrinsic friction velocity dependence is a function of displacement for simulated gouge. Before further discussion of the implications of this analysis it is important to recognize that the experiments of Marone *et al.* [1990] and those of this study were conducted under significantly different conditions, of which the following is a partial list: (1) quartz versus granite, (2) 190-50 versus 25 MPa normal stress, (3) ~10% versus ~20% porosity, (4) wet drained versus dry, (5) 4 versus 1-mm-thick gouge, (6) triaxial versus rotary shear testing geometry, and (7) different measure of dilatancy, volume versus thickness. Therefore it is not entirely reasonable to expect the two studies to agree. However, considering the experiments of this study alone, the failure of (8) or (10) to quantitatively explain the differences in friction veloc-

ity dependence between gouges and bare surfaces implies that the term represented by $d\mu_{ss}^T / d \ln V$ in (8) or (10) is not equal to the friction velocity dependence of bare surfaces.

Other sources of positive frictional velocity dependence. A conclusion, evident from Figure 9, is that additional velocity-dependent processes must accompany dilation in gouges, which do not operate on bare surfaces, to increase the friction velocity dependence and stabilize slip. This conclusion is not surprising if we consider the micromechanical processes which are possibly present during deformation of gouge. According to the view we have adopted in (7), the strength of gouge is the sum of two components: (1) the intrinsic frictional strength μ^T , which is the stress necessary to slide grains past one another, and (2) the dilatational stress $dL / d\delta$, which is the shear stress required to thicken the layer against the normal stress during shear strain. Two significant observations relevant to use of this equation in fault mechanics were made by Mandl *et al.* [1977]. First, the term identified as μ^T in (7) can change with strain for granular materials which undergo both interparticle slip and grain fracture with shear, such as the simulated gouges in the current study. Thus, for such materials, μ^T is not truly an intrinsic material property. Mandl *et al.* [1977] interpret observed variations in μ^T with displacement as resulting from changes in the relative amounts of interparticle slip to grain fracture. Second, dilatancy changes sympathetically with μ^T . Mandl *et al.* [1977] interpret this correlation to result from variations in the amount of grain fracture: dilatancy changes because grain fracture is a dilatant process.

Both of the observations of Mandl *et al.* [1977] are consistent with the variations in μ^T and dilatancy with displacement in the experiments of the current study. To illustrate the relationship between μ^T and dilatancy, (7) can be used to determine μ^T from μ^A and $dL / d\delta$; throughout the experiments, $|dL / d\delta| < 0.01$ and at displacements beyond 30 mm, $|dL / d\delta|$ is generally < 0.002 . This contribution to μ^A is sufficiently small that for simplicity, we can consider observed variations in μ^A as representative of variations in μ^T . Variations in μ^T are large as a function of displacement in our simulated gouges (Figure 5a), particularly within the first 100 mm of displacement as deformation first becomes localized and subsequently becomes more distributed. By analogy with the results of Mandl *et al.* [1977], these variations in friction reflect changes in the micromechanisms of deformation within the gouge; as the micromechanisms change, so must $d\mu_{ss}^T / d \ln V$ provided the mechanisms do not have identical velocity dependence. Although we do not have the detailed microstructural evidence necessary to determine precisely how micromechanical processes vary with displacement, the observations convincingly demonstrate that as μ^T changes, $d\mu_{ss}^T / d \ln V$ also changes (Figures 5 and 9). A related argument was suggested by Biegel *et al.* [1989], who attributed more positive friction velocity dependence of gouge to increased grain fracture.

In (7) the processes responsible for dilatancy are not identified, nor does the dilatancy change the energy of the system. Since we observe covariation of $d\mu_{ss}^T / d \ln V$ (the only energy dissipating term in (8)) with $d(dL / d\delta)_{ss} / d \ln V$, it is reasonable to conclude that dilatancy itself involves (or results from) processes which change the energy of the system. These processes may include inter-particle slip or the creation of surface area by grain fracture. Both processes are liable to be velocity dependent, which is consistent with the observed correlation between $d\mu_{ss}^T / d \ln V$ and $d(dL / d\delta)_{ss} / d \ln V$ (Figure 6). A unifying explanation of the observations in our study of simulated gouge is that the intrinsic friction, the net thickness change, the velocity dependence of dilation rate, and the intrinsic friction velocity dependence corre-

late, because, contrary to the prediction of (7), dilatancy alters (or results from processes which alter) the energy dissipation or the stored energy of the system.

Conclusions

In this study we have conducted experiments to displacements as large as 400 mm on initially bare surfaces and 1-mm-thick layers of simulated Westerly granite at 25 MPa and 25°C to determine the friction velocity dependence as a function of displacement. Initially bare surfaces show velocity weakening and the friction velocity dependence does not vary with displacement. The friction velocity dependence of simulated gouge is velocity strengthening at short displacements but decreases with displacement to ~40 mm where it is velocity weakening; subsequently, it increases, becoming velocity strengthening/neutral again by 100 mm, and remains velocity strengthening/neutral to 400 mm displacement. The displacement dependence of the friction velocity dependence in simulated gouge correlates with displacement dependencies of friction, of the velocity dependence of dilation rate, and with the degree of localization of deformation. Localized deformation is accompanied by low strength, negative friction velocity dependence, and a small velocity dependence of dilation rate. Distributed deformation is stronger, has neutral to positive friction velocity dependence, and a larger velocity dependence of dilation rate. The observed velocity dependence of dilation rate in gouge is consistent with the interpretation of *Marone and Kilgore* [1993]; its magnitude indicates the degree of localization, or the total volume of gouge actively undergoing shear.

The correlation of friction, the friction velocity dependence, the velocity dependence of dilation rate, and the degree of localization in simulated gouge suggests that all quantities are related, but the observations do not allow the independent variables to be identified. However, the observations do suggest that the progressive localization and delocalization with displacement are determined by the fault strength, not the friction velocity dependence, and that the localization is encouraged by boundary conditions which may be unique to the experimental geometry.

At large displacements the texture of simulated gouges continues to change with displacement, indicating that true textural equilibrium has not been reached. The preferred mode of deformation of simulated gouge at large displacement is distributed; thus the friction velocity dependence of gouge differs from initially bare surfaces of the same composition at the largest displacements tested. Attempts to explain quantitatively the difference between bare surfaces and simulated gouges using theory which accounts for a contribution to gouge friction velocity dependence from the velocity dependence of dilation rate fail, in contrast to the results of *Marone et al.* [1990]. A possible explanation for this failure is that the theory used does not permit processes involved in dilatancy to change the energy of the system except through frictional heating.

Appendix A: Boundary Conditions in Rotary Shear

A cross section of our samples shows an important boundary condition of the Teflon jacket geometry, the jacket split (Figure A1a). The sliding jacket has four parts, inner and outer jackets which separate into upper and lower halves. The upper halves are fixed with the upper sample, and the lower halves rotate with the

lower grip. Consequently, a large slip discontinuity is introduced at the boundary between upper and lower jacket halves and the gouge. This boundary condition is similar to a mode III crack and may have a significant effect on the stresses in the vicinity of the jacket split. It requires that strain is localized in the gouge adjacent to the jacket split. This boundary condition suggests that these rotary shear gouge samples are more liable to localize than those with a simple shear boundary (triaxial) or a free boundary (direct shear).

This tendency to localize plays an important role in determining whether localized slip is favored at the upper or the lower gouge-rock interface in granite gouge experiments. It is very difficult to prepare experiments where the jacket split is exactly at the center of the gouge at the outset of an experiment. The procedures used uniformly resulted in the jacket split being closer to the lower gouge-rock interface at least at the outset of an experiment. The stress concentration in the gouge adjacent to the jacket split is sufficient to cause the basal shear zone to nucleate on the boundary closer to the jacket split. (Figure A1b)

Other features introduced by the jacket are corner effects (Figure A1b). At the gouge-rock-jacket interface there is a "dead zone" caused by the combined shielding of the gouge and jacket. The gouge in these corners is relatively undeformed. Thus the deformation in our gouges is never precisely a homogeneous shear. In a more ideal case, where the jacket split is precisely in the center of the gouge, the strength of the gouge-rock interface is indistinguishable from any plane parallel to it, and the gouge has

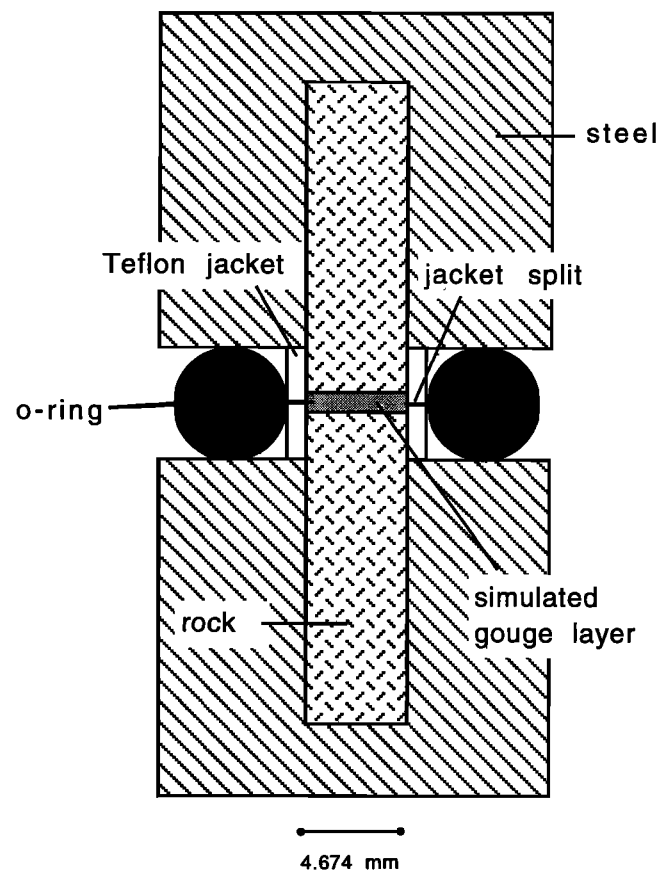


Figure A1a. Cross section of jacket geometry. Jacket split is a fully localized boundary condition which influences the degree of localization in rotary shear experiments (see text).

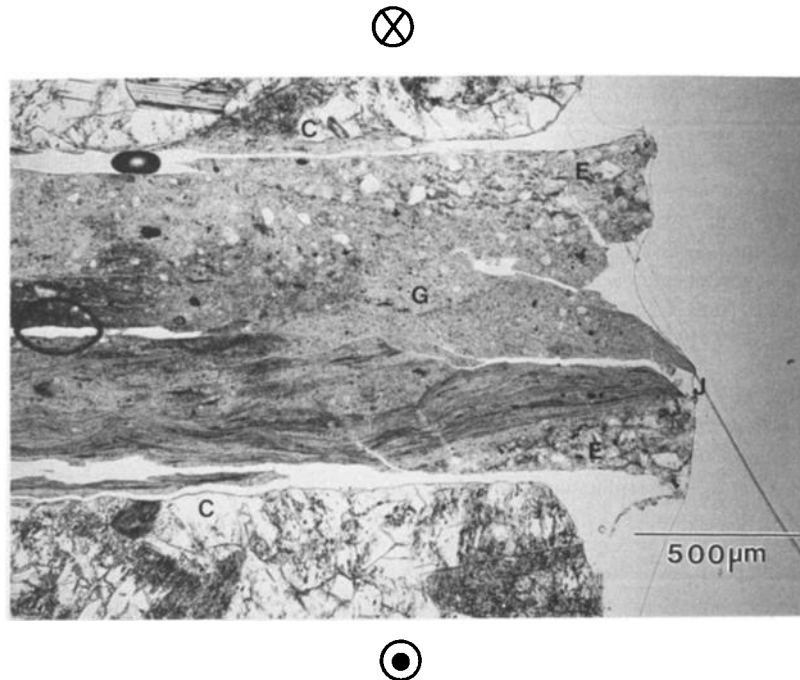


Figure A1b. Optical photomicrograph of a radially cut thin section of simulated granite gouge after 403 mm displacement. The sense of shear is top away from the reader. The total gouge thickness is roughly 1 mm. The forcing blocks (C) became detached from the gouge zone during the thin section preparation, which resulted in the gouge zone (G) being offset to the right of the blocks. The "corner effect" (E) introduced by jacket boundary conditions is evident at the right-hand base and right-hand top of the gouge layer where the gouge is coarse and relatively undeformed. The position of the split between the two halves of the sliding jacket (J) encourages localized deformation, the jackets have been removed and are not shown. A weak gouge-rock interface and the jacket split cause deformation to localize in a concave upward shaped shear zone.

homogeneous frictional properties which do not vary with displacement, homogeneous deformation would occur within a crudely elliptical region, the apices of which are the jacket splits. In our nonideal case the jacket split causes deformation to be concentrated near the initially weak lower gouge-rock interface, and displacement dependent frictional properties of the gouge lead to spatially and temporally varying strength contrasts within the gouge. Differences in the position of the jacket split in nominally identical experiments may be important even at large displacement and may influence the degree of localization, perhaps resulting in some of the variability in friction velocity dependence measurements for gouge (Figures 6 and B2).

Appendix B: Data for All Experiments

For completeness, we have included friction, friction velocity dependence, and change in length of the loading column ΔL where $\Delta L = L - L_0$ and L_0 is the starting column length, versus δ data for all experiments used in this study. These are shown in Figures B1 (initially bare surfaces) and B2 (simulated gouges). For initially bare surfaces, there are subtle differences between experiments. For example, FR94 and FR103 have a very similar loading slope $d\mu / d\delta$ over the first 10 mm of slip, while FR121 has a significantly lower μ . These differences probably derive from differences in surface preparation. Differences in strength between nominally identical, initially bare surfaces seen at smaller displacement were found to correlate with surface roughness measurements by *Biegel et al.* [1992]. Such differences may

be responsible for the difference in sign of the friction velocity dependence during the "run-in" stage (first 15 mm of slip). FR94 and FR103 are initially velocity strengthening, and FR121 is velocity weakening (Figure B1).

Differences in initial conditions become less important at large displacements. Strength and velocity dependencies of FR94 and FR121 are very similar at large displacements, having undergone an almost identical set of velocity step tests (Figure B1). The principal differences in the testing procedure of FR121 and FR94 are periods of unloading of shear stress in FR94 at 230 and 372 mm (most obvious as permanent offsets in ΔL Figure A2c). Because the data shown in these plots are averaged over 100 μm in δ , complete unloads of shear stress rarely appear to be complete unloads. FR103 was slid to ~ 93 mm before a series of "hold" tests and low-velocity (0.1-0.001 $\mu\text{m/s}$) step tests were performed. The spikes on the friction and ΔL records beyond 93 mm for FR103 are the results of "hold" tests. The large stress drops are due to low shear stress holds. The deviations of ΔL during FR103 from the trends exhibited by ΔL measured during the other two experiments may be associated with differences in deformation history.

For simulated gouges the differences between nominally identical experiments are more pronounced. All experiments show the same general strength features: a peak friction, a strength minimum, and a restrengthening at displacements greater than 50 mm. However, individual experiments are quite different in detail. For example, FR95 undergoes a second loss of strength starting at 220 mm. The loss of strength follows an unload of shear stress.

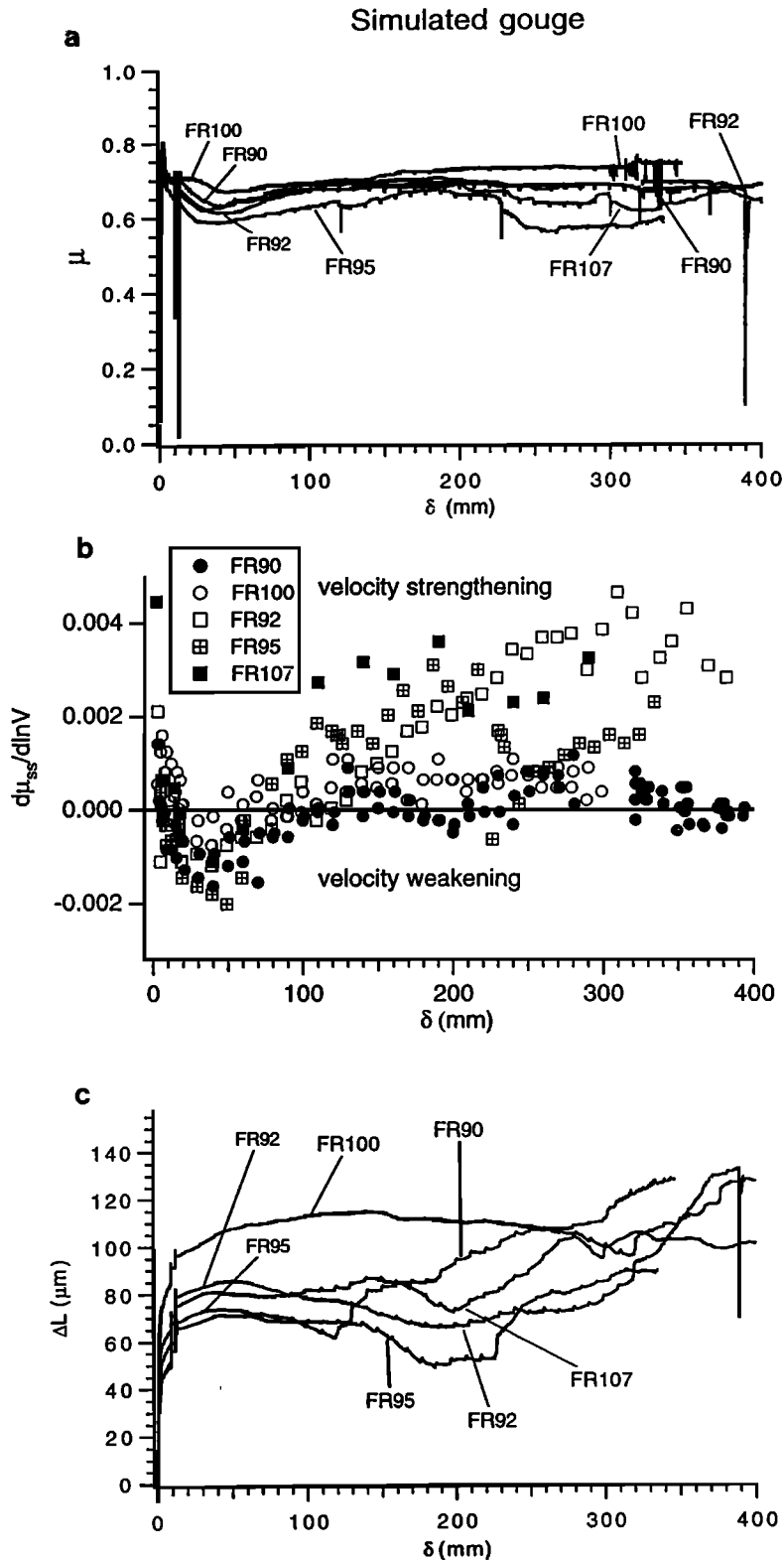


Figure B1. Friction, friction velocity dependence, and sample column length change versus displacement for three initially bare surfaces. (a) Friction. (b) Friction velocity dependence. Friction velocity dependence in this summary plot may be slightly different than shown in Figure 4. These values were reduced from run records, while those in the paper are determined from inversions of the computerized data. The results of inversions and the data reduction procedure both depend to some degree on the total displacement following the change in sliding velocity over which the method is applied. The choice of total displacement following the velocity step is not consistent between the two methods. (c) Sample column length change (change of thickness of the fault zone).

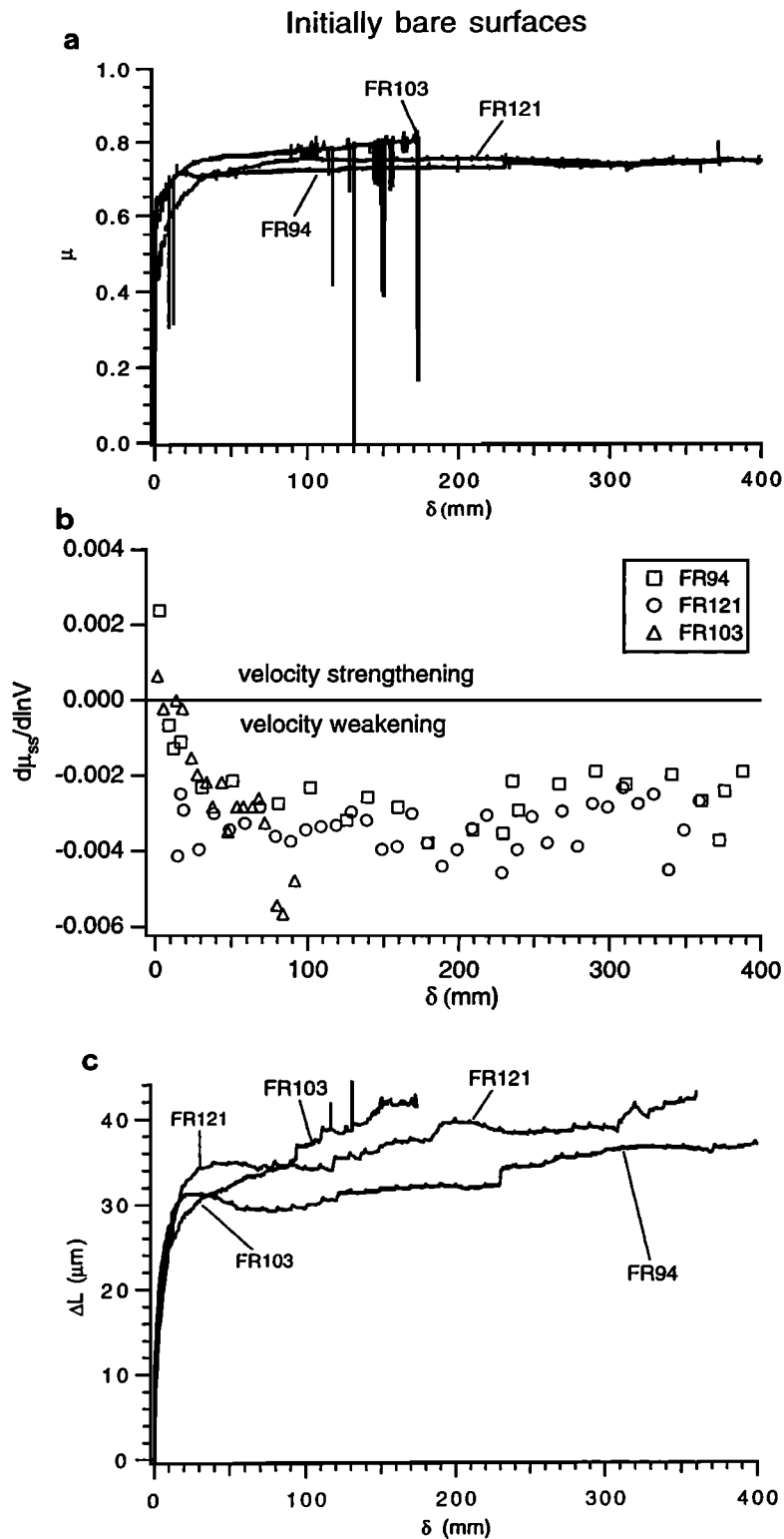


Figure B2. Friction, friction velocity dependence, and sample column length change versus displacement for five simulated gouges. (a) Friction. (b) Friction velocity dependence. Friction velocity dependence in this summary plot may be slightly different than shown in Figures 5 and 6, for the same reasons as stated in the Figure B2 caption. (c) Sample column length change (change of thickness of the fault zone).

Corresponding to this change in load history, there is a large drop in the friction velocity dependence following the unload which accompanies the loss of strength. This correlation between strength and friction velocity dependence is another illustration of the relationship between strength and friction velocity depen-

dence seen at all displacements in simulated gouge experiments. We interpret the second loss of strength and the associated reduction in friction velocity dependence in FR95 as a localization brought on by the unload. The unload is most obvious on the ΔL vs δ plot and corresponds to a permanent compaction of $\sim 10 \mu\text{m}$.

Acknowledgments. Thanks to referees C. Marone, F. Chester, associate editor A. Kronenberg, and to J. Tullis for reviews which vastly improved the content and presentation of this article. N.M.B. benefited greatly from discussions of gouge friction with C. Marone and L. Reinen. This study was supported by USGS grants 14-08-0001-G-1364 / 1775 and 1434-93-G-2278 / 94-G-2422 and NSF grants EAR-8407991 / 8816791 / 9206649 / 9220005 / 9317038.

References

- Aydin, A., Small faults formed as deformation bands in sand-stone, *Pure Appl. Geophys.*, 116, 913-930, 1978.
- Aydin, A., and A. M. Johnson, Development of faults as zones of deformation bands and as slip surfaces in sandstone, *Pure Appl. Geophys.*, 116, 931-942, 1978.
- Beeler, N. M., Experimental and theoretical studies of rock friction and earthquake rupture, Ph.D. thesis, Brown Uni., Providence, R.I., 1995.
- Beeler, N. M., and T. E. Tullis, Implications of Coulomb plasticity for the velocity dependence of experimental faults, *Pure Appl. Geophys.*, 144, 251-276, 1995.
- Biegel, R. L., C. G. Sammis, and J. H. Dieterich, The frictional properties of a simulated gouge with a fractal particle distribution, *J. Struct. Geol.*, 11, 827-846, 1989.
- Biegel, R. L., W. Wang, C. H. Scholz, and G. N. Boitnott, Micromechanics of rock friction, 1, Effects of surface roughness on initial friction and slip hardening in Westerly granite, *J. Geophys. Res.*, 97, 8951-8964, 1992.
- Bishop, A. W., Discussion of shear characteristics of a saturated slit, measured in triaxial compression, *Geotechnique*, 4, 43-45, 1959.
- Blanpied, M. L., D. A. Lockner, and J. D. Byerlee, Frictional slip of granite hydrothermal conditions, *J. Geophys. Res.*, 100, 13,045-13,064, 1995.
- Brace, W. F., and J. D. Byerlee, Stick-slip as a mechanism for earthquakes, *Science*, 153, 990-992, 1966.
- Brace, W. F., A. S. Orange, and T. R. Madden, The effect of pressure on the electrical resistivity of water-saturated crystalline rocks, *J. Geophys. Res.*, 70, 5669-5678, 1965.
- Byerlee, J. D., Friction of rocks, *Pure Appl. Geophys.*, 116, 615-626, 1978.
- Byerlee, J. D., and J. C. Savage, Coulomb plasticity within the fault zone, *Geophys. Res. Lett.*, 19, 2341-2344, 1992.
- Byerlee, J., and R. Summers, A note on the effect of fault gouge thickness on fault stability, *Int. J. Rock Mech. Min. Sci. Geomech. Abstr.*, 13, 35-36, 1976.
- Dieterich, J. H., Time-dependent friction and the mechanics of stick slip, *Pure Appl. Geophys.*, 116, 790-806, 1978.
- Dieterich, J. H., Modeling of rock friction, 1, Experimental results and constitutive equations, *J. Geophys. Res.*, 84, 2161-2168, 1979.
- Dieterich, J. H., Constitutive properties of faults with simulated gouge, in *Mechanical Behavior of Crustal Rocks*, *Geophys. Monogr. Ser.* vol. 24, edited by N. L. Carter et al., 103-120, AGU, Washington, D.C., 1981.
- Edmond, J. M., and M. S. Paterson, Volume changes during the deformation of rocks at high pressures, *Int. J. Rock Mech. Min. Sci.*, 9, 161-182, 1972.
- Gu, J., J. R. Rice, A. L. Ruina, and S. Tse, Stability of frictional slip for a single degree of freedom elastic system with non-linear rate and state dependent friction, *J. Mech. Phys. Solids*, 32, 167-196, 1984.
- Hobbs, B. E., A. Ord, and C. Marone, Interpretation of rate dependent frictional behavior in terms of rate dependent Coulomb constitutive laws, in *Dynamic Behavior of Rock Joints*, *Proc. Int. Symp. on Rock Joints*, edited by N. R. Barton and O. Stephansson, pp. 435-445, Balkema, Rotterdam, 1990.
- Linker, M. F., and J. H. Dieterich, Effects of variable normal stress on rock friction: observations and constitutive equations, *J. Geophys. Res.*, 97, 4923-4940, 1992.
- Lockner, D. A., and J. D. Byerlee, How geometrical constraints contribute to the weakness of mature faults, *Nature*, 363, 250-252, 1993.
- Lockner, D. A., R. Summers, and J. D. Byerlee, Effects of temperature and sliding rate on frictional strength of granite, *Pure Appl. Geophys.*, 124, 445-469, 1986.
- Logan, J. M., M. Friedman, N. G. Higgs, C. Dengo, and T. Shimamoto, Experimental studies of simulated gouge and their application to studies of natural fault gouge, in *Analysis of Actual Fault Zones in Bedrock*, edited by R. C. Speed and R. V. Sharp, *U.S. Geol. Surv. Open file Rep. 79-1239*, 276-304, 1979.
- Mandl, G., L. N. J. De Jong, and A. Maltha, Shear zones in granular materials, *Rock Mech.*, 9, 95-144, 1977.
- Marone, C., Micromechanics of rate- and state-dependent friction in simulated gouge, *Eos Trans. AGU*, 74, 295-296, 1993.
- Marone, C., and B. Kilgore, Scaling of the critical slip distance for seismic faulting with shear strain in fault zones, *Nature*, 362, 618-621, 1993.
- Marone, C., and C. H. Scholz, The depth of seismic faulting and the upper transition from stable to unstable slip regimes, *Geophys. Res. Lett.*, 15, 621-624, 1988.
- Marone, C., C. B. Raleigh, and C. H. Scholz, Frictional behavior and constitutive modeling of simulated fault gouge, *J. Geophys. Res.*, 95, 7007-7025, 1990.
- Marone, C., C. H. Scholz, and R. Bilham, On the mechanics of earthquake afterslip, *J. Geophys. Res.*, 96, 8441-8452, 1991.
- Marone, C., B. E. Hobbs, and A. Ord, Coulomb constitutive laws for friction: Contrasts in behavior for distributed and localized shear, *Pure Appl. Geophys.*, 139, 195-214, 1992.
- Morrow, C., and J. Byerlee, Experimental studies of compaction and dilatancy during frictional sliding on faults containing gouge, *J. Struct. Geol.*, 11, 815-825, 1989.
- Power, W. L., T. E. Tullis, and J. D. Weeks, Roughness and wear during brittle faulting, *J. Geophys. Res.*, 98, 15,268-15,278, 1988.
- Rice, J. R., and A. L. Ruina, Stability of steady frictional slipping, *J. Appl. Mech.*, 50, 343-349, 1983.
- Ruina, A. L., Slip instability and state variable friction laws, *J. Geophys. Res.*, 88, 10,359-10,370, 1983.
- Scott, D. E., C. J. Marone, and C. G. Sammis, The apparent friction of granular gouge in sheared layers, *J. Geophys. Res.*, 99, 7231-7246, 1994.
- Solberg, P., and J. D. Byerlee, A note on the rate sensitivity of frictional sliding of Westerly granite, *J. Geophys. Res.*, 89, 4203-4205, 1984.
- Tullis, T. E., Rock friction constitutive behavior from laboratory experiments and its implications for an earthquake prediction field monitoring program, *Pure Appl. Geophys.*, 126, 555-588, 1988.
- Tullis, T. E., and J. D. Weeks, Constitutive behavior and stability of frictional sliding of granite, *Pure Appl. Geophys.*, 124, 384-414, 1986.
- Weeks, J. D., and T. E. Tullis, High-resolution measurement of displacement in rock friction experiments, *Eos Trans. AGU*, 73, 565, 1992.
- Wong, T., Y. Gu, T. Yanagidani, and Y. Zhao, Stabilization of faulting by cumulative slip, in *Fault Mechanics and Transport Properties in Rocks*, edited by B. Evans and T. Wong, pp. 109-133, Academic, San Diego, Calif., 1992.

N. M. Beeler and M. L. Blanpied, U.S. Geological Survey, 345 Middlefield Road, MS 977, Menlo Park, CA 94025. (e-mail: nbeeler@isdml.wr.usgs.gov; mblanpied@isdml.wr.usgs.gov)

T. E. Tullis, Department of Geological Sciences, Brown University, Providence, RI 02912. (e-mail: Terry_Tullis@brown.edu)

J. D. Weeks, Wavemetrics, Inc., P.O. Box 2088, Lake Oswego, OR 97035.

(Received March 20, 1995; revised November 13, 1995; accepted January 31, 1996.)